CHEMICAL REVIEWS

REVIEW

pubs.acs.org/CR

Nonadiabatic Quantum Chemistry—Past, Present, and Future

David R. Yarkony*

Department of Chemistry, Johns Hopkins University, Baltimore, Maryland 21218, United States

CONTENTS

1. BACKGROUND AND DEFINITIONS

This review discusses the current state of the art of theoretical descriptions, and computational treatments, of nonadiabatic processes; reviews how the field got to this point; and suggests, with little likelihood of success, directions along which the field may evolve. The field has grown rapidly in the past two decades so that it is impossible to touch on, let alone describe, all areas affected by nonadiabatic processes. What I have attempted to do is provide more than a casual description of several broadly defined directions in computational nonadiabatic chemistry and provide citations or less detailed discussions of other work in those areas.

1.1. Some History

In a nonadiabatic process the description of nuclear motion involves more than one Born−Oppenheimer potential energy surface. The theory of nonadiabatic chemical reactions goes back to at least 1932, when London's classic work, "On the Theory of Nonadiabatic Chemical Reactions", appeared.[1] London observed that the simplest examples of such reactions include[2] charge exchange [$Ar + N^+ \leftrightarrow Ar^+ + N$]; energy transfers [$Hg' + Na \leftrightarrow Hg + Na'$ (activation, stimulated fluorescence, etc.]; and formation of ion molecules from atoms [$Na + Cl_2 \leftrightarrow NaCl + Cl$, etc.]. The current list is much longer!

Although the theory of nonadiabatic reactions goes back nearly to the advent of quantum mechanics, our understanding of the mechanism of these processes has changed dramatically in recent years with the appreciation that intersections of potential energy surfaces, particularly conical intersections,[3−5] defined carefully below, play a significant role in such processes.

In retrospect, the previous obscurity of conical intersections may appear surprising because their importance in nonadiabatic processes, including radiationless decay, was appreciated early on. A 1937 paper[6] authored by E. Teller and entitled "The Crossing of Potential Energy Surfaces" was concerned with

Special Issue: 2012 Quantum Chemistry

Received: April 15, 2011
Published: November 03, 2011

"whether the molecules can get from a higher potential energy surface to a lower one, transforming in this way electronic excitation energy into kinetic energy and finally into heat." Using an extension of the 1-dimensional analysis of Zener,[7] Teller showed that conical intersections may lead to rapid radiationless decay. As in many modern day dynamics treatments, in Teller's analysis, nuclear motion was treated classically whereas the electrons were described using wave function techniques.

A consequence of Teller's observation that conical intersections are engines of nonadiabatic transitions is that electronic structure techniques that locate and characterize conical intersections could provide qualitative insights into the potential outcome of nonadiabatic processes, in the absence of actual nuclear dynamics. However, Teller's insights into the significance of conical intersections were ahead of their time. The significance of conical intersections in nonadiabatic processes would not be appreciated for an additional half century.

1.2. Conical Intersections, Derivative Couplings and the Diabatic Representation

To describe a nonadiabatic process mathematically, the total wave function for the N^{at} nuclei (coordinates $\mathbf{R}_j$, $j = 1 - N^{at}$) and the N^{el} electrons (coordinates $\mathbf{r}_j$, $j = 1 - N^{el}$), which satisfies the time-independent Schrödinger equation

$$(H^T(\mathbf{r},\mathbf{R}) - E_k^T)\Psi_K^T(\mathbf{r},\mathbf{R}) = 0 \tag{1a}$$

is expanded as

$$\Psi_K^T(\mathbf{r},\mathbf{R}) = \sum_{J=1}^{N^{state}} \Psi_J^{e,a}(\mathbf{r},\mathbf{R})\chi_J^K(\mathbf{R}) \tag{1b}$$

where

$$\begin{aligned} H^{\mathrm{T}}(\mathbf{r},\mathbf{R}) &= \sum_{l=1}^{N^{at}} -\frac{1}{2M_l}\nabla_l^2 + H^{\mathrm{e}}(\mathbf{r},\mathbf{R}) \\ &\equiv T^{\mathrm{nuc}} + H^{\mathrm{e}}(\mathbf{r},\mathbf{R}) \end{aligned} \tag{1c}$$

and the adiabatic electronic wave functions $\Psi_J^{e,a}$ are eigenfunctions of the standard (Coulomb) electronic Hamiltonian, $H^e(\mathbf{r},\mathbf{R})$, that is,

$$[H^e(\mathbf{r},\mathbf{R}) - E_J^e(\mathbf{R})]\Psi_J^{e,a}(\mathbf{r},\mathbf{R}) = 0 \tag{2}$$

Inserting eq 1b into eq 1a and taking the dot product with $\Psi_M^{e,a}$ gives

$$\begin{aligned} &(T^{nuc} + E_M^e(\mathbf{R}) + K_{M,M}(\mathbf{R}) - E_K^T)\chi_M^K(\mathbf{R}) \\ &= \sum_{J\neq M}\left[\sum_{l=1}^{N^{at}} \frac{\boldsymbol{f}_l^{M,J}(\mathbf{R})}{M_l}\cdot\nabla_l - K_{M,J}(\mathbf{R})\right]\chi_J^K(\mathbf{R}) \end{aligned} \tag{3a}$$

where

$$\begin{aligned} \boldsymbol{f}_l^{M,J}(\mathbf{R}) &= <\Psi_M^{e,a}(\mathbf{r},\mathbf{R})|\nabla_l\Psi_J^{e,a}(\mathbf{r},\mathbf{R})>_{\mathbf{r}} \\ \mathbf{f}^{M,J}(\mathbf{R}) &= <\Psi_M^{e,a}(\mathbf{r},\mathbf{R})|\nabla\Psi_J^{e,a}(\mathbf{r},\mathbf{R})>_{\mathbf{r}} \end{aligned} \tag{3b}$$

so that $\mathbf{f}^{M,J}(\mathbf{R}) = [\boldsymbol{f}_1^{M,J}(\mathbf{R}), \boldsymbol{f}_2^{M,J}(\mathbf{R}), ..., \boldsymbol{f}_{N^{at}}^{M,J}(\mathbf{R})]$ and

$$K_{M,J}(\mathbf{R}) = <\Psi_M^{e,a}(\mathbf{r},\mathbf{R})|T^{\mathrm{nuc}}\Psi_J^{e,a}(\mathbf{r},\mathbf{R})>_{\mathbf{r}} \tag{3c}$$

Here $\mathbf{f}^{M,J}(\mathbf{R})$ is the derivative coupling and $K_{M,M}$ is the adiabatic or Born−Oppenheimer diagonal correction.[8−16] Note that $\mathbf{f}^{M,J}(\mathbf{R})$ is an antisymmetric matrix, that is, $\mathbf{f}^{M,J}(\mathbf{R}) = -\mathbf{f}^{J,M}(\mathbf{R})$ whose elements are $3N^{at}$ dimensional vectors. For clarity, we note that, as indicated in eq 3b and the text that follows, because the subscript l in $\boldsymbol{f}_l^{M,J}(\mathbf{R})$ refers to an atom, each $\boldsymbol{f}_l^{M,J}(\mathbf{R})$ is a three-component vector. Thus $\boldsymbol{f}_l^{M,J}(\mathbf{R})$ denotes three components of the $3N^{at}$ dimensional vector $\mathbf{f}^{M,J}(\mathbf{R})$. Using a complete set of adiabatic states in eq 3c gives

$$K_{M,M}(\mathbf{R}) = -\sum_{l,N}\frac{\boldsymbol{f}_l^{M,N}(\mathbf{R})\cdot\boldsymbol{f}_l^{N,M}(\mathbf{R})}{2M_l} \tag{3d}$$

Equation 3a represents a system of coupled equations for the nuclear motion, with the coupling provided by $\mathbf{f}_L^{M,J}$ and $K_{M,J}$. In general the contribution $\mathbf{f}_L^{M,J}$ is much larger than that of $K_{M,J}$. The vicinity of points of intersection of the potential energy surfaces, that is, regions where $E_M^e(\mathbf{R}^x) \approx E_N^e(\mathbf{R}^x)$, are clearly regions of particular interest. Note that, when the intersection is a conical one, $K_{M,M}(\mathbf{R}) \approx K_{N,N}(\mathbf{R})$ for $\mathbf{R} \approx \mathbf{R}^x$ and $K_{M,M}(\mathbf{R}^x) = K_{N,N}(\mathbf{R}^x) = +\infty$. The behavior of $K_{M,M}(\mathbf{R})$ near $\mathbf{R}^x$ produces a node in the adiabatic wave functions at $\mathbf{R}^x$.

To simplify eq 3a, the diabatic basis is introduced. The diabatic basis is obtained from the adiabatic basis by a unitary transformation:

$$\Psi_K^{e,d}(\mathbf{r},\mathbf{R}) = \sum_L \Psi_L^{e,a}(\mathbf{r},\mathbf{R})U_{L,K}(\mathbf{R}) \tag{4a}$$

and is designed to remove the coupling terms on the right-hand side of eq 3a. Rigorous diabatic states should have vanishing derivative couplings, that is, they should satisfy

$$<\Psi_M^{e,d}(\mathbf{r},\mathbf{R})|\nabla\Psi_K^{e,d}(\mathbf{r},\mathbf{R})>_{\mathbf{r}} = 0 \tag{4b}$$

which becomes

$$\begin{aligned} <\Psi_M^{e,d}(\mathbf{r},\mathbf{R})|\nabla\Psi_K^{e,d}(\mathbf{r},\mathbf{R})>_{\mathbf{r}} &= \sum_{J,J'} U_{J',M}(\mathbf{R})[\mathbf{f}^{J',J}(\mathbf{r},\mathbf{R})U_{J,K}(\mathbf{R}) \\ &\quad + \delta_{J,J'}U_{J',M}(\mathbf{R})\nabla U_{J,K}(\mathbf{R})] \\ &= (\mathbf{U}^\dagger\mathbf{f}\mathbf{U})_{M,K} + (\mathbf{U}^\dagger\nabla\mathbf{U})_{M,K} = 0 \end{aligned} \tag{4c}$$

so

$$\mathbf{f}\mathbf{U} + \nabla\mathbf{U} = 0 \tag{4d}$$

This innocent looking equation has been the subject of much discussion. For diatomic molecules that have only 1 internal coordinate, eq 4d is a differential equation and is readily integrated provided the derivative couplings $\mathbf{f}^{I,J}$ are available.[17,18] However, for molecules with more than one internal degree of freedom, eq 4d is a partial differential equation. Baer observed that eq 4d can be solved by path integration, but he also noted that the integral would only be path-independent provided a curl condition on the derivative coupling was satisfied.[19−21] Mead and Truhlar[22] further analyzed the situation and traced the failure of the curl condition to derivative couplings outside the space included in eq 4a. Thus, they concluded that a rigorous diabatic basis only exists in the trivial case in which a complete basis is included in eq 4a. This result is consistent with an earlier observation by Smith.[17] For this reason approximate diabatic bases are referred to as quasi-diabatic. For the remainder of this review, we will suppress the attribute quasi.

dx.doi.org/10.1021/cr2001299 |Chem. Rev. 2012, 112, 481–498

If rigorous diabatic bases did exist, eq 3a would have the form

$$(T^{\mathrm{nuc}} + H^{d}_{M,M}(\mathbf{R}) - E^{T}_{K})\chi^{K,d}_{M}(\mathbf{R}) = \sum_{J\neq M} H^{d}_{M,J}\chi^{K,d}_{J}(\mathbf{R}) \quad (5a)$$

where

$$\Psi^{T}_{K}(\mathbf{r},\mathbf{R}) = \sum_{J=1}^{N^{\mathrm{state}}} \Psi^{e,d}_{J}(\mathbf{r},\mathbf{R})\chi^{K,d}_{J}(\mathbf{R}) \quad (5b)$$

and

$$H^{d}_{J,K}(\mathbf{R}) = <\Psi^{e,d}_{J}(\mathbf{r},\mathbf{R})|H^{e}|\Psi^{e,d}_{K}(\mathbf{r},\mathbf{R})>_{\mathbf{r}} \quad (5c)$$

Because of the incredible simplicity of eq 5a compared to eq 3a, much effort has been devoted to the determination of approximate[23−30] or even the most[31,32] diabatic basis. It is fairly routine to use eq 5a regardless of the quality of the diabatic representation. This point is discussed further in section 2.

1.3. Classifying Conical Intersections: Symmetry Considerations

We now turn to the classification of points of conical intersection. It is useful to partition conical intersections; here we restrict to intersections of two states, into three groups: symmetry-required intersections, accidental symmetry-allowed intersections, and accidental same-symmetry intersections.[4] For symmetry-required intersections the specification that the molecule has a particular point group symmetry is sufficient to guarantee the degeneracy of the electronic states, that is, the electronic states are members of a two-dimensional irreducible representation. For accidental symmetry-allowed intersections the two states carry distinct one-dimensional irreducible representations. No degeneracies are guaranteed, but they may be found by changing only one totally symmetric nuclear coordinate. Actually the restriction of the distinct representations to one-dimensional representations is unnecessary but is used here because we have restricted the discussion to two state intersections. Finally for accidental same-symmetry intersections two coordinates must be changed to locate a degeneracy.

The existence of accidental same-symmetry conical intersections was recognized early on. In 1929 J. von Neumann and E. Wigner published their classic work "On the Behavior of Eigenvalues in Adiabatic Processes".[33] They observed that for real symmetric matrices it suffices to be able to change two (five) real parameters to make two (three) eigenvalues of an $N \times N$ real symmetric Hamiltonian degenerate. Since for diatomics, which have only one internal coordinate, no crossings of states of the same symmetry are permitted, this result is (unfortunately) frequently referred to as the noncrossing rule.

1.4. Prevalence of Conical Intersections

Despite the rigorous results of von Neumann and Wigner and the insights of Teller, until ∼1990, because most molecules do not have any point group symmetry, let alone high enough symmetry to possess symmetry-required degeneracies, there was some skepticism that conical intersections were sufficiently prevalent to warrant general attention. The situation in this period was described in a 1974 review, entitled "Physical Basis of Qualitative MO Arguments in Organic Photochemistry".[34] In this review J. Michl wrote, "While in principle the various hypersurfaces can cross as the nuclear configuration is varied along various paths this is a relatively uncommon occurrence and along most paths such crossings, even if intended, are more or less strongly avoided." This opinion, with regard to conical intersections not required or allowed by symmetry, was prevalent, although not universally held,[35,36] until the early 1990s. Indeed in the early 1970s some confusion about the validity[37] of the noncrossing rule itself arose, although those questions were ultimately set aside.[38,39]

In the last 20 years conical intersections have gone from an arcane theoretical construct to an essential concept in explaining nonadiabatic processes.[40−42] In that period there have been two key advances in the electronic structure tools for dealing with conical intersections: (i) algorithms to locate conical intersections[43−47] and (ii) formal and computational tools to characterize conical intersections.[48−51]

1.5. Locating and Characterizing Conical Intersections

There are basically two classes of algorithms for locating conical intersections, those that exploit the derivative couplings[43−45] and those that do not.[46] In this review we focus on the former since the tools used in those searches are also applicable to the characterization of conical intersections.

First, we discuss some electronic structure results. The adiabatic electronic state is expanded in a large configuration state function (CSF) basis, $\psi_{\alpha}(\mathbf{r},\mathbf{R})$, $\alpha = 1, ..., N^{\mathrm{CSF}}$, as

$$\Psi^{e,a}_{J}(\mathbf{r},\mathbf{R}) = \sum_{\alpha=1}^{N^{\mathrm{CSF}}} c^{J}_{\alpha}(\mathbf{R})\psi_{\alpha}(\mathbf{r},\mathbf{R}) \quad (6)$$

where the $\mathbf{c}^{J}$ satisfy

$$[\mathbf{H}^{\mathrm{CSF}}(\mathbf{R}) - \mathbf{I}E^{a}_{J}(\mathbf{R})]\mathbf{c}^{J}(\mathbf{R}) = 0 \quad (7a)$$

and $H^{\mathrm{CSF}}_{\alpha,\beta}(\mathbf{R}) = \langle\psi_{\alpha}(\mathbf{r},\mathbf{R})|H^{e}|\psi_{\beta}(\mathbf{r},\mathbf{R})\rangle_{\mathbf{r}}$. Then define

$$\mathbf{h}^{M,N}(\mathbf{R}) \equiv \mathbf{c}^{M}(\mathbf{R})^{\dagger}\nabla\mathbf{H}^{\mathrm{CSF}}(\mathbf{R})\mathbf{c}^{N}(\mathbf{R}) \quad (7b)$$

where $\nabla H^{\mathrm{CSF}}_{\alpha,\beta}(\mathbf{R}) = \nabla\langle\psi_{\alpha}|H^{e}(\mathbf{r},\mathbf{R})|\psi_{\beta}\rangle_{\mathbf{r}}$. Also note that the derivative or nonadiabatic coupling is given by

$$\mathbf{f}^{I,J}(\mathbf{R}) = \langle\Psi^{e,a}_{I}(\mathbf{r};\mathbf{R})|\nabla|\Psi^{e,a}_{J}(\mathbf{r};\mathbf{R})\rangle_{\mathbf{r}} = {}^{CI}\mathbf{f}^{I,J}(\mathbf{R}) + {}^{CSF}\mathbf{f}^{I,J}(\mathbf{R}) \quad (8)$$

where

$${}^{CI}\mathbf{f}^{I,J}(\mathbf{R}) = \sum_{\alpha} c^{I}_{\alpha}(\mathbf{R})\nabla c^{J}_{\alpha}(\mathbf{R}) = \frac{\mathbf{h}^{I,J}(\mathbf{R})}{E^{a}_{J}(\mathbf{R}) - E^{a}_{I}(\mathbf{R})} \quad (9a)$$

and

$${}^{CSF}\mathbf{f}^{I,J}(\mathbf{R}) = \sum_{\alpha} c^{I}_{\alpha}(\mathbf{R})\langle\psi_{\alpha}|\nabla\psi_{\beta}\rangle_{\mathbf{r}}c^{J}_{\beta}(\mathbf{R}) \quad (9b)$$

The $\mathbf{h}^{M,N}$ are efficiently obtained[49,52] using analytic gradient techniques.[53]

Two state degeneracies of eq 7a are degeneracies in a space of dimension N^{CSF}. Most discussions of two state conical intersections rely on 2×2 matrices. The relation between these two perspectives is established using degenerate perturbation theory.[54] It was shown[49] that in the vicinity of $\mathbf{R}^{x}$ where a two state degeneracy of 7a for states I, J exists, that is, for $\mathbf{R}$ near $\mathbf{R}^{x}$ or

dx.doi.org/10.1021/cr2001299 |Chem. Rev. 2012, 112, 481–498

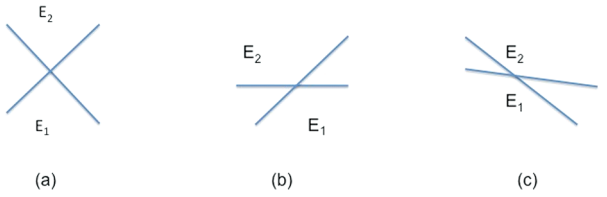

Figure 1. Peaked (a), intermediate (semilevel) (b), and sloped (c) crossings after ref 48.

$\mathbf{R} = \mathbf{R}^x + \delta\mathbf{R}$, the eigenenergies of 7a can be obtained from the following eigenvalue problem:

$$\left[(E_J^a(\mathbf{R}^x) + \mathbf{s}^{I,J}\cdot\delta\mathbf{R})\begin{pmatrix}1 & 0\\ 0 & 1\end{pmatrix} + \begin{pmatrix}-\mathbf{g}^{I,J}(\mathbf{R}^x)\cdot\delta\mathbf{R} & \mathbf{h}^{I,J}(\mathbf{R}^x)\cdot\delta\mathbf{R}\\ \mathbf{h}^{I,J}(\mathbf{R}^x)\cdot\delta\mathbf{R} & \mathbf{g}^{I,J}(\mathbf{R}^x)\cdot\delta\mathbf{R}\end{pmatrix}\right]\begin{pmatrix}\bar{c}_1^K(\mathbf{R})\\ \bar{c}_2^K(\mathbf{R})\end{pmatrix} = E_K^{d,a}(\mathbf{R})\begin{pmatrix}\bar{c}_1^K(\mathbf{R})\\ \bar{c}_2^K(\mathbf{R})\end{pmatrix} \tag{10a}$$

where

$$E_K^{d,a}(\mathbf{R}) = E_J^a(\mathbf{R}^x) + \mathbf{s}^{I,J}\cdot\delta\mathbf{R} \pm [(\mathbf{g}^{I,J}\cdot\delta\mathbf{R})^2 + (\mathbf{h}^{I,J}\cdot\delta\mathbf{R})^2]^{1/2} \tag{10b}$$

$E_J^a(\mathbf{R}^x) = E_I^a(\mathbf{R}^x)$, $K = \pm$, the energy difference gradient, $\mathbf{g}^{IJ}$, is given by

$$\mathbf{g}^{I,J} = (\mathbf{h}^{J,J} - \mathbf{h}^{I,I})/2 \tag{11a}$$

and the average energy gradient, $\mathbf{s}^{IJ}$, is given by

$$\mathbf{s}^{I,J} = (\mathbf{h}^{J,J} + \mathbf{h}^{I,I})/2 \tag{11b}$$

When $E_K^{d,a}(\mathbf{R})$ is plotted along the directions $\mathbf{g}^{IJ}$ and $\mathbf{h}^{IJ}$, it has the appearance of a double cone. Vertical sections through possible double cones are shown in Figure 1. Thus, at $\mathbf{R}^x$ the vectors $\mathbf{s}^{IJ}(\mathbf{R}^x)$, $\mathbf{g}^{IJ}(\mathbf{R}^x)$, and $\mathbf{h}^{IJ}(\mathbf{R}^x)$ describe the local topography of the intersecting potential energy surfaces. Note that directions orthogonal to $\mathbf{g}^{IJ}(\mathbf{R}^x)$ and $\mathbf{h}^{IJ}(\mathbf{R}^x)$ contribute only at second or higher order to eq 10. Further it can be shown that at a conical intersection $\mathbf{g}^{IJ}(\mathbf{R}^x)$ and $\mathbf{h}^{IJ}(\mathbf{R}^x)$ can be chosen[27] such that $\mathbf{g}^{IJ}(\mathbf{R}^x) \perp \mathbf{h}^{IJ}(\mathbf{R}^x)$. Consequently, it is useful to define a coordinate system known as intersection adapted coordinates,[48] composed of two unit vectors $\hat{\mathbf{x}} = \mathbf{g}^{IJ}(\mathbf{R}^x)/\|\mathbf{g}^{IJ}(\mathbf{R}^x)\|$, $\hat{\mathbf{y}} = \mathbf{h}^{IJ}(\mathbf{R}^x)/\|\mathbf{h}^{IJ}(\mathbf{R}^x)\|$, which comprise the branching plane, and $3N^{at} - 8$ mutually orthogonal directions, which span the intersection or seam space. In the seam space the degeneracy is lifted starting at no lower than second order, depending on the curvature[50,55] of the seam space. It is also convenient to define $s_x^{IJ}(\mathbf{R}^x) = \mathbf{s}^{IJ}\cdot\hat{\mathbf{x}}$ and $s_y^{IJ}(\mathbf{R}^x) = \mathbf{s}^{IJ}\cdot\hat{\mathbf{y}}$. For minimum energy conical intersections, these are the only nonvanishing components of $\mathbf{s}^{IJ}$.

We are now in a position to make a rigorous definition of a conical intersection of two electronic states. $\mathbf{R}^x$ is a point of conical intersection if and only if $E_I^a(\mathbf{R}^x) = E_J^a(\mathbf{R}^x)$ and neither $\mathbf{g}^{IJ}(\mathbf{R}^x)$ nor $\mathbf{h}^{IJ}(\mathbf{R}^x)$ is zero.

The local topography of conical intersections has been carefully studied by Ruedenberg's group, in a work denoted *AXR*.[48] At $\mathbf{R}^x$ *AXR* identify three main topographies referred to as peaked, intermediate, and sloped intersections. These topographies are pictured in Figure 1.

The peaked intersection has the character of a vertical double cone in that the lower (upper) surface decreases (increases) in all directions from the intersection. For these cones $s_x^{IJ} = s_y^{IJ} = 0$. For the intermediate and sloped intersections, s_x^{IJ}, $s_y^{IJ} \neq 0$. In the intermediate, semilevel crossing $s_x^{IJ} = \|\mathbf{g}^{IJ}\| \equiv g^{IJ}$ whereas in the sloped crossing $s_x^{IJ} \gg g^{IJ}$. In these cones of rotation, similar relations hold for s_y^{IJ} and $\|\mathbf{h}^{IJ}\| \equiv h^{IJ}$. A related classification[56] based on the $\mathbf{s}^{IJ}$, $\mathbf{g}^{IJ}$, and $\mathbf{h}^{IJ}$, which explicitly takes account of the potentially different magnitudes of g^{IJ} and h^{IJ}, has also been proposed. This classification defines three quantities: pitch, $\rho^{IJ} = [(g^{IJ})^2 + (h^{IJ})^2]^{1/2}$; asymmetry, $\Delta = [((g^{IJ})^2 - (h^{IJ})^2)/((g^{IJ})^2 + (h^{IJ})^2)]^{1/2}$; and tilt (s_x^{IJ}, s_y^{IJ}).

The above linear analyses have been extended to include second-order terms. Robb and co-workers characterize the topography of a point of conical intersection within the seam or intersection space using a Hessian matrix projected into the intersection space.[47,50] In this way points of conical intersection are characterized in terms of standard potential energy surface notions, that is, minima, maxima, and saddle points. Their analysis also leads to an extension of the linear intersection adapted coordinates to a set of curvilinear coordinates defined through second order.[50,57] The use of this analysis is discussed further in section 2 below.

The set of all points of conical intersection forms a connected seam in the space of nuclear coordinates. It represents a generalized line in nuclear coordinate space and is a subspace of dimension $3N^{at} - 8$ in a space of dimension $3N^{at} - 6$. There is potentially more than one such (locally) connected seam.[58,59] But whether such seams necessarily meet and how they meet remains an open question.[60] There are certainly instances when two distinct seams intersect. We refer to such points as confluences.[61−63] Confluences are not points of conical intersection by the above definition since one of g^{IJ} or h^{IJ} is 0.

2. CURRENT STATE OF THE ART

In this section current work in the area of computational nonadiabatic chemistry is summarized. While the work summarized is representative of that being done in this field, the summary is not exhaustive and I apologize in advance for omissions.

2.1. Conical Intersections and Radiationless Decay

Radiationless decay of electronically excited states is a fundamental issue in nonadiabatic chemistry. The example discussed below, taken from the work of Köppel and co-workers[64] and denoted *GTGK*, illustrates some of the electronic structure issues associated with locating conical intersections and determining the mechanism and outcome of excited state radiationless decay.

2.1.1. Radiationless Decay of Furan (C_4H_4O). Fast radiationless decay provides prima facie evidence of the involvement of conical intersections. In this section we overview the detailed study of the mechanism of the photoinduced ring-opening for furan, by *GTGK*. The process is summarized on the abscissa in Figure 2.

The goals of this overview are to illustrate the role of conical intersections in fast radiationless processes and to describe issues in the associated electronic structure treatments and in the representation of the resulting potential energy surfaces and their interactions. The states and their interactions were described using high-quality equations of motion coupled cluster single and double (EOM-CCSD) techniques[65] based on cc-pVDZ+ basis sets.

dx.doi.org/10.1021/cr2001299 |*Chem. Rev.* 2012, 112, 481–498

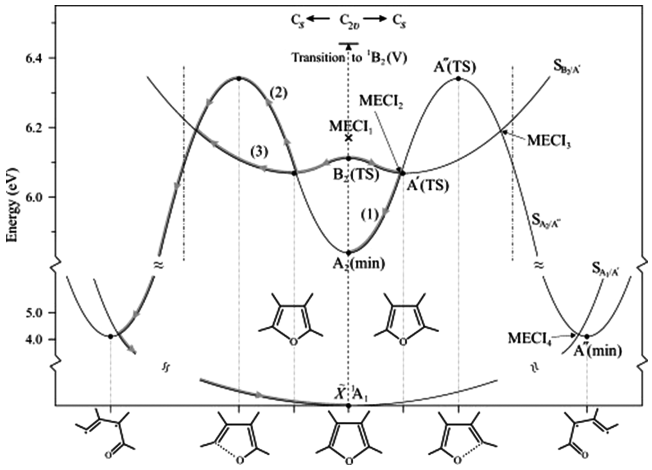

Figure 2. Cross-sections of the S_0, S_1, S_2 potential energy surfaces along the ring-opening reaction coordinate. Stationary points are denoted by dots, minimum energy conical intersections $MECI_2$−$MECI_4$ are indicated by arrows, and $MECI_1$ is indicated by a cross. The molecular structure is sketched for each stationary point. Three relaxation/decay paths 1−3 after vertical transition to S_2 are suggested. The region of the potential energy surfaces between the two dash-dotted lines was fit using polyspherical coordinates.
Reprinted with permission from ref 64. Copyright 2010 American Institute of Physics.

GTGK performed their calculations in C_{2v} or C_s symmetry. In addition to the cost savings attributable to exploiting point group symmetry in the electronic structure calculations, with point group symmetry the conical intersections considered are accidental symmetry allowed, rather than accidental same-symmetry intersections. *GTGK* observed that the highly accurate EOM-CCSD methods can have trouble with accidental same-symmetry conical intersections because of the nonhermitian character of the EOM eigenvalue problem.[66] This problem does not occur in the multireference configuration interaction approach used to define $\mathbf{g}^{IJ}$ and $\mathbf{h}^{IJ}$ in section 1.

Two excited states are of interest, S_2 and S_1. At the C_{2v} equilibrium geometry of the ground state S_0, these states are 3s Rydberg for $S_1(^1A_2)$ and valence for $S_2(^1B_2)$ in character. The analyzed photodissociation process originates with the strong $S_2 \leftarrow S_0$ absorption. A transition state S_2(TS) (labeled ^{1}A″(TS) in Figure 2) was determined that leads from the Franck−Condon region to a highly nonadiabatic region characterized by an S_2/S_1 energy-minimized conical intersection ($MECI_3$) and an S_1/S_0 energy-minimized conical intersection ($MECI_4$). $MECI_4$ is found to be in close proximity to the ring-opened structure denoted A″(min) in Figure 2. *GTGK* also describe $MECI_1$ and $MECI_2$, which lead to the ground state, avoiding the ring-opened structure. On the basis of the electronic structure results summarized in Figure 2, *GTGK* describe several feasible radiationless decay paths, including (i) path 1 radiationless decay to $S_1(^1A_2)$ through conical intersections, $MECI_1$, or $MECI_2$, which are in the Franck−Condon region, and (ii) two ring-opening paths, paths 2 or 3. The electronic structure treatment is essential to establish the possible mechanisms. Additional qualitative mechanistic information could be obtained from a determination of the $\mathbf{s}^{I,J}$, $\mathbf{g}^{I,J}$, and $\mathbf{h}^{I,J}$ vectors (see section 2.6.1). However, *GTGK* observe that, in this case, reliable determination of the probability of the ring-opening and its mechanism requires nonadiabatic dynamical calculations.

To enable dynamics studies, *GTGK* have constructed partial representations of the ab initio potential energy surfaces for planar furan, using polyspherical[67] coordinates. There are overall 15 polyspherical coordinates that describe all in-plane configurations of furan; however, to reduce the complexity, approximations were introduced to reduce the representation to 11 polyspherical coordinates, which were divided into active and harmonic degrees of freedom. For the active coordinates, a two-dimensional energy grid was constructed for each potential energy surface. With respect to the remaining nine coordinates, the surfaces were represented using Taylor series up to second-order terms. The resulting eleven-dimensional model surfaces were tested against results of the ab initio calculations. These tests showed that the model surfaces reproduce fairly well those for all the states ranging from C_{2v} symmetrical configurations to C_s configurations in the vicinity of the A″(TS) transition state and including points of minimum energy conical intersection. The successful modeling of these portions of the ab initio potential energy surfaces provides a good basis for dynamical calculations. Note that the use of C_s symmetry means that for the regions considered the electronic states can be considered diabatic. The issue of constructing coupled potential energy surfaces to study nonadiabatic dynamics is an important one in the field of nonadiabatic quantum chemistry, and it is to this matter that we now turn.

2.2. Diabatic States and the Representation of Adiabatic Potential Energy Surfaces and Their Couplings

The solution of the nonadiabatic dynamics problem requires the determination of ab initio electronic structure data, either in its adiabatic form, energies, energy gradients, and derivative couplings, or in the diabatic representation, where equivalent information is carried in the matrix elements of the diabatic Hamiltonian $\mathbf{H}^d$. This data can be provided as required, directly from ab initio calculations. In this case, to generate diabatic data, a transformation to diabatic states that is independent of the order in which the nuclear geometries are selected is required. The determination of the ab initio data in this manner can be quite costly and results uniformly in the use of more approximate treatments of the electronic structure than would otherwise be possible. Instead, in favorable circumstances, the ab initio data can be provided by functional forms. In this approach a lower density of higher-quality ab initio data is used to define a functional form, which then provides the electronic structure data as needed.

Because strongly coupled adiabatic surfaces, particularly those involving conical intersections, are difficult to represent directly, as in the example in section 2.1, diabatic representations are used. The representation of ab initio determined coupled adiabatic state potential energy surfaces using coupled diabatic state Hamiltonians, $\mathbf{H}^d$, is a well-studied problem in nonadiabatic chemistry of significant current interest.[68−76] Within this general class of problems, it is useful to identify two subsets, descriptions of bound molecules and descriptions of dissociative species. Representations of bound molecules can be done in a set of nonredundant nuclear coordinates. Representations of dissociative potential energy surfaces and their couplings require more general coordinate representations.

Much of the work in this area is based on the vibronic coupling model, introduced by Köppel, Domcke, and Cederbaum over a quarter century ago[3,5] and updated by those workers[77,78] and others.[68,70,79−81] Also notable are the perturbation theory-based

dx.doi.org/10.1021/cr2001299 |*Chem. Rev.* 2012, 112, 481–498

work of Mead, Truhlar, Varandas, and co-workers;[82,83] the direct diabatization schemes of Nakamura and Truhlar,[84,85] based on the earlier work of Atchity and Ruedenberg;[86] the regularized diabatization procedure of Köppel et al.;[28] the block diabatization method of Pacher, Cederbaum, and Köppel;[24,87] the Shepard interpolation-based method of Collins, Evenhuis, and co-workers;[72,88,89] and methods specific to triatomic molecules with nontrivial point group symmetry.[90,91]

Recently we have introduced[74,75,92] a promising approach for using a diabatic Hamiltonian, $\mathbf{H}^d$ to represent N^{state} ab initio determined potential energy surfaces coupled by conical intersections. This approach represents an extension of the vibronic coupling model, noted above, and can treat both bound and dissociative electronic states. A principal and unique advantage of this approach is that it includes derivative couplings in the fitting procedure so that not only is it quantifiably diabatic but it is maximally diabatic in a least-squares sense. This representation provides a removable[22] approximation to the derivative coupling,

In this approach, the diabatic Hamiltonian $\mathbf{H}^d$, eq 5c, is an $N^{\text{state}} \times N^{\text{state}}$ matrix whose elements are functions of internal coordinates. The adiabatic energies ($E_J^{d,a}$) and wave functions ($\mathbf{e}^J$) are determined from the electronic Schrödinger equation

$$[\mathbf{H}^d - \mathbf{I}E_J^{d,a}]\mathbf{e}^J = 0 \tag{12}$$

2.2.1. H^d for Bound States. Our bound-state methodology originally considered only a single, albeit arbitrary, point of conical intersection.[80] However, based on Lagrange multiplier techniques developed in ref 74, we have extended that approach, determining an $\mathbf{H}^d$ that can reproduce both the ab initio determined locus and the local topography of a seam of conical intersection.[76] This is enabled by an analysis of a conical intersection in orthogonal[27] intersection adapted coordinates[48] together with the above noted Lagrange multiplier constraint capabilities. The matrix elements of $\mathbf{H}^d$ are given by

$$\begin{aligned} H^d_{\alpha,\beta}(\mathbf{Q}) = {} & E^a_\alpha(\mathbf{Q}^0)\delta_{\alpha,\beta} + \sum_{k=1}^{N^{\text{int}}} V_k^{(1),\alpha,\beta} w_k \\ & + 1/2 \sum_{k,l=1}^{N^{\text{int}}} V_{k,l}^{(2),\alpha,\beta} w_k w_l \\ & + 1/3 \sum_{k,l,m=1}^{N^{\text{int}}} V_{k,l,m}^{(3),\alpha,\beta} w_k w_l w_m + \ldots \end{aligned} \tag{13}$$

The $\mathbf{V}^{(n),\alpha,\beta}$ reflect the symmetry properties of the molecule. For the bound molecules, the symmetry group is the point group of the molecule at the origin $\mathbf{Q}^0$. For bound molecules the $\mathbf{w}$ are simply a set of N^{int} nonredundant internal coordinates.[93]

2.2.2. H^d for Dissociative States. For dissociative states the monomials in eq 13 are more complicated, owing to the need to describe arbitrarily large displacements. Further the symmetry group in question is the complete nuclear permutation inversion (CNPI) group.[94−96] In this case it is useful to view $\mathbf{H}^d$ as expanded in a set of basis matrices

$$\mathbf{H}^d = \sum_{n=1}^{N^f} \sum_{\alpha\le\beta=1}^{N^{\text{state}}} V^{(n),\alpha,\beta} f_{n,\alpha,\beta} \mathbf{M}^{(\alpha,\beta)} \tag{14}$$

Here $\mathbf{M}^{(\alpha,\beta)}$ is an $N^{\text{state}}(N^{\text{state}}+1)/2$ matrix whose (α,β) element is equal to 1, with all of the other elements equal to 0. The $f_{n,\alpha,\beta}$ are constructed from primitive f_n, monomials of the form:

$$f_n = \prod_{m=1}^{3} \prod_{i<j} (w_m(r_{i,j}))^{\alpha^{(n)}_{m,i,j}} \prod_{(i,j,k,l)} (w_4^{i,j,k,l})^{\beta^{(n)}_{i,j,k,l}} \tag{15}$$

It should be noted that in eq 15, (n) is a label, not an exponent, but $\alpha^{(n)}_{m,i,j}$ and $\beta^{(n)}_{i,j,k,l}$ are exponents. Here $r_{i,j} = |\mathbf{R}^i - \mathbf{R}^j|$, $1 \le i,j \le N^{\text{at}}$ and $\mathbf{R}^i$ are the atom-centered Cartesian coordinates of the ith N^{at} nuclei and (i,j,k,l) denotes the allowed combinations of four atoms. Four distinct functions, w_j, $j = 1-4$, of the internuclear separations are used:

- Exponential functions $w_1(r_{i,j}) = e^{-s_1(r_{i,j} - r_{i,j}{}^a)}$ (16a)
- Gaussian functions $w_2(r_{i,j}) = e^{-s_2(r_{i,j} - r_{i,j}{}^b)^2}$ (16b)
- Reciprocal functions $w_3(r_{i,j}) = e^{-s_3(r_{i,j} - r_{i,j}{}^c)}/(r_{i,j} + r_{i,j}{}^d)$ (16c)
- Dot−cross product functions

$$w_4^{i,j,k,l} = \mathbf{r}_{i,j} \times \mathbf{r}_{i,k} \cdot \mathbf{r}_{i,l} / |r_{i,j} r_{i,k} r_{i,l} r_{j,k} r_{j,l} r_{k,l}|^{1/2} \tag{16d}$$

The dot−cross product functions are due to Collins and coworkers.[72] The remaining functions were suggested by the single adiabatic potential energy surface work of Braams and Bowman.[97] Note that these functions form a redundant set. The appropriate symmetry is imposed on the monomials using standard projection operator techniques, giving $f_{n,\alpha,\beta}$.

2.2.3. Determining H^d. The expansion coefficients $V^{(n),\alpha,\beta}$ are determined by setting, for each geometry chosen, the $\mathbf{H}^d$ predicted values of the energies, gradients, and derivative couplings to be equal to the ab initio determined values. The following issues guide the construction of the algorithm for determining the $\mathbf{V}$:

(1) Because data at a large number of nuclear configurations is used, the number of equations exceeds the number of unknowns and the $\mathbf{V}$ must be solved in a least-squares sense.

(2) It is sometimes necessary to require some of the ab initio data to be exactly reproduced. For example, energy difference must be exactly zero at a point of conical intersection, to ensure that proper intersection-adapted coordinates can be constructed; the branching plane vectors $\mathbf{g}^{I,J}$ and $\mathbf{h}^{I,J}$ also need to be exactly reproduced, so that the residual coupling is finite at a point of intersection. It is also desirable that energies and gradients be reproduced at critical points to ensure correct topology of $\mathbf{H}^d$. Lagrange multipliers (λ_j) are used to require the corresponding equations be solved exactly. Points at which these constraints are applied are called nodes.

(3) Some of the $\mathbf{V}$ may not be well-defined by the available ab initio data. This problem is overcome by introducing a diagonal or flattening term, $\mathbf{V}^\dagger\mathbf{t}\mathbf{V}$, where $\mathbf{t}$ is a positive definite diagonal matrix.

(4) Some of the data have lower importance than others and can be fitted with less accuracy. Examples include energies and gradients at energetically inaccessible geometries and derivative couplings at points where the states are well separated. In these cases, the corresponding equations will be weighted according to their importance.

dx.doi.org/10.1021/cr2001299 |Chem. Rev. 2012, 112, 481–498

To sum up, coefficients **V** are obtained by solving a linear, equality constrained, rank-deficient weighed pseudolinear least-squares problem. The problem is solved self-consistently using weighted normal equations with Lagrange multipliers and a diagonal flattening term.[74] The final equations are reported in ref 74. The bound-state version of this algorithm has been used with considerable success recently.[76,98−101] Preliminary results for the dissociative state version are encouraging.[74,75]

2.3. Nuclear Dynamics for Electronically Nonadiabatic Processes

It goes without saying that the electronic structure aspects of any nonadiabatic process are only half the problem. The nuclear motion problem must be solved to determine the measured quantities. After years of being relegated to an arcane theoretical concept, it is now part of the conventional wisdom that conical intersections are a significant player in the world of fast nonadiabatic processes. Their presence makes nonadiabatic nuclear dynamics computationally demanding. For nonadiabatic processes the nuclear motion problem is important even if one is only seeking mechanistic inferences. This point was emphasized in our introductory example in section 2.1. For a conical intersection, low energy is not sufficient to establish its importance or even its involvement in a nonadiabatic process. In a nonadiabatic photochemical process, the wave packet evolves on the excited-state potential energy surface until the region of a conical intersection is reached. The question of which region of the seam of conical intersection is encountered in a particular nonadiabatic event is a key issue, because different regions of the seam may well lead to different outcomes. Two factors help decide where on the seam the nonadiabatic event occurs, the initial conditions, and the topography of the excited-state surface. To address these qualitative issues as well as the details of a nonadiabatic process, a treatment of the nuclear motion problem is required.

In this section we identify, by reference, several significant techniques for treating nonadiabatic dynamics. Nonadiabatic dynamics is intrinsically quantum mechanical because a change of electronic states is involved. However, the nuclear motion can be treated quantum mechanically, classically, or semiclassically. Time-dependent quantum mechanical treatments include the ab initio multiple spawning (AIMS) approach,[102] the multiconfiguration time-dependent Hartree (MCTDH)[103−105] method and its direct formulation based on Gaussian wave packets,[106,107] and the matching pursuit split operator Fourier transform method.[108] Classical treatments of the nuclear motion are also available in the trajectory surface-hopping method.[109] This approach is much more cost-effective than the aforementioned fully quantum methods but has its limitations, because, for example, it does not correctly account for zero point energy. For a careful analysis of potential issues with the surface-hopping method, see ref 110. Quantum mechanical methods based on the Ehrenfest principle are also available, but they may suffer from the fact that the nuclear motion takes place on an average potential energy surface. One way to avoid the limitations of the Ehrenfest treatment and the surface-hopping approach while maintaining the computational advantages of classical mechanics is the semiclassical initial-value problem approach, advocated by Miller and co-workers.[111,112]

2.4. Nonadiabatic Effects near Surfaces and Interfaces

It was pointed out by Wodtke, Tully, and Auerbach[113] that nonadiabatic processes are preeminent at metal surfaces. Semiconductor interfaces provide similar challenges. As explained in section 2.4.2 below, the existence of a high density of energetically accessible states is key to the prevalence of nonadiabatic effects in metals. A similar situation presents itself in semiconductors. In this section, we illustrate these effects.

2.4.1. Semiconductor Interfaces. Electron transfer (ET) at semiconductor surfaces drives important applications including photocatalysis, photoelectrolysis, and solar energy production. One example of this situation is the nonadiabatic photon-induced electron transfer from an anchored electron donor to semiconductor acceptor. This problem has been studied by Prezhdo and co-workers.[114,115] Both adiabatic and nonadiabatic mechanisms are available for the ET, and the competition between these mechanisms is an important issue.

To illustrate, we overview a recent study of a dye−semiconductor system.[115] The electronic structure of the dye−semiconductor system and the adiabatic dynamics are simulated by ab initio molecular dynamics (MD), whereas the nonadiabatic effects are incorporated by a quantum-classical mean-field approach. In the adiabatic mechanism, the coupling between the dye and the semiconductor is large, and ET occurs through a transition state along the reaction coordinate that involves a concerted motion of nuclei. During adiabatic transfer, the electron remains in the same adiabatic state that continuously changes its localization from the dye to the semiconductor along the reaction coordinate. Nonadiabatic effects decrease the amount of ET that happens at the transition state but open up a new channel involving direct transitions from the dye into the semiconductor that can occur at any nuclear configuration (not necessarily a conical intersection). Nonadiabatic transfer becomes important when the dye−semiconductor coupling is weak, and when perturbation theory is applicable, the rate of transfer is proportional to the density of acceptor states.

An example of this type of nonadiabatic process is the alizarin−TiO_2 interface, where photoinduced electron transfer was observed in 6 fs. The alizarin−TiO_2 system has recently been studied by the Prezhdo group,[115] in a paper denoted *DSP*. In contrast to the typical Grätzel cell systems,[116] where the excited state of molecular donors are in resonance with a high density of semiconductor conduction band acceptor states, in TiO_2 sensitized with alizarin the molecular photoexcited state is at the edge of the conduction band, an inference supported by high level ab initio analysis of the optical absorption spectrum. *DSP* resolved a controversy regarding the origin of the ultrafast ET by showing that, although ultrafast nonadiabatic transfer is possible, the observed ET proceeds mostly adiabatically. Their simulation indicates that following photoexcitation the electron is injected into a localized surface state within 8 fs and spreads into the bulk on a 100-fs or longer time scale. The molecular architecture seen in the alizarin−TiO_2 system permits efficient electron injection into the edge of the conduction band by an adiabatic mechanism without the energy loss associated with injection high into the conduction band by a nonadiabatic process.

2.4.2. Metal Surfaces. Nonadiabatic processes involving molecules, particularly open-shell molecules, interacting with metal surfaces are inherently different from those involving gas-phase molecules. This, Tully and co-workers,[117] in a work denoted *RST*, observe, is a consequence of the large number of closely spaced states in the vicinity of the Fermi level, provided by the metal. Consider Figure 3, taken from *RST*. When $O(^3P)$ approaches a closed-shell species, here H_2, the interaction is unfavorable and the ^3P state splits as indicated in Figure 3a.

dx.doi.org/10.1021/cr2001299 |*Chem. Rev.* 2012, 112, 481–498

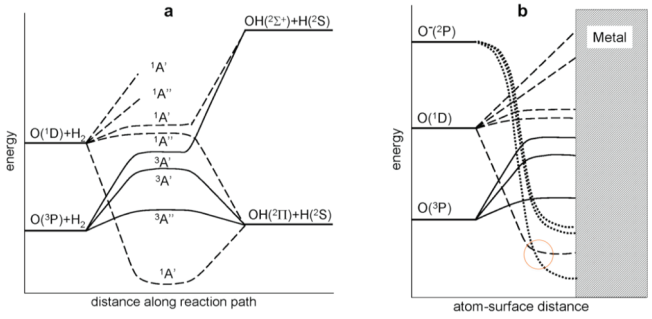

Figure 3. Schematic representation of multiple potential energy surfaces and their crossing that can arise when an open-shell species, here an oxygen atom or ion, interacts with a molecule (plate a) or a metal (plate b).
Reprinted with permission from ref 117. Copyright 2009 American Chemical Society.

The components of the ^{3}P state cross a strongly bound ^{1}A′ state correlating asymptotically with O(^{1}D) + H_2, as well as with ground-state water in the interacting region. However, the probability of a nonadiabatic transition, an intersystem crossing from the triplet manifold to the singlet manifold, is small, since the spin−orbit coupling is weak. The possibility of oxygen changing its spin-state from triplet to singlet changes dramatically when H_2 is replaced by, for example, a gold surface. Here two things change. Gold makes available a continuum of orbitals in the vicinity of the Fermi level. It also impacts the size of the spin−orbit interaction through the heavy atom effect.[118−121] In the heavy atom effect the molecular orbitals of a low atomic number (Z) atom or molecule (here oxygen) are responsible for the spin−orbit coupling. Because Z is small, the spin−orbit coupling is weak. However, as the oxygen approaches the metal surface, the metal orbitals overlap with those of oxygen and the spin−orbit coupling matrix element acquires a contribution from the high Z metal, which does not reflect the spin-state of the metal. This increase in the spin−orbit interaction facilitates a change in the spin-state of the oxygen and an overall change in the spin-state of the oxygen−metal system. An additional, more generalizable, mechanism applicable in the O(^{3}P) + gold surface is noted by *RST*. In this mechanism the spin-state of the oxygen−metal system is unchanged but the spin-state of the oxygen and of the metal moieties each individually change. In this case, near the singlet−triplet intersection the oxygen flips a spin in its 2p shell going from O(^{3}P) to O(^{1}D) while the metal does a particle-to-hole singlet−triplet excitation near the Fermi level. This creates an electron−hole pair (EHP) on the metal. This scenario is not feasible in Figure 3a because of the high cost of flipping a spin on H_2. This simultaneous spin flip is equivalent to a simultaneous two-electron transfer in which an electron with one spin is transferred from near the Fermi level to the metal while an electron with the opposite spin is transferred to an unoccupied near Fermi level orbital of the metal. Head-Gordon and Tully have shown[122,123] that this creation of EHPs can be described as molecular friction. From the above analysis it is seen that this EHP or molecular friction is able to drive a variety of configurational changes in the electronic state of a molecule approaching a metal surface.

Also shown in Figure 3b (see red circle) is the transient negative ion mechanism, introduced by Gadsuk.[124] In this use of Figure 3b, the metal is assumed to have one fewer electron when the oxygen is negatively charged. Thus, a neutral molecule interacting with a metal surface may, in the course of its interaction, create a temporary transient negative ion state. This negative ion−positive metal arrangement causes energy transfer between the molecule and the metal. We first point out that the intersection in Figure 3b may be an avoided or a conical intersection. Further its location and energy may be modified by the creation of EHP.

These changes in the state of the molecule interacting with the metal surface provide for a variety of energy-transfer processes. The correct description of these processes requires both accurate description of the relevant potential energy surfaces and their interactions and the nonadiabatic dynamics.

The dynamics of NO scattering from Au(111) illustrates the previously described processes and the competition between adiabatic and nonadiabatic alternatives.[125] Tully and co-workers observe that for NO (v = 0) adiabatic and nonadiabatic simulations generally agree and are in good accord with experimental results.[126] For NO (v = 2) the adiabatic and nonadiabatic results differ significantly, with the nonadiabatic results being in better accord with the experiment. Tully and co-workers explain this in terms of deeper excursions into the ionic regions of Figure 3, where nonadiabatic effects increase. For NO (v = 15) the differences between the adiabatic and nonadiabatic results are even more striking, with trapping of NO on the surface, somewhat surprisingly, enhanced by nonadiabaticity, an observation carefully explained in ref 117.

2.5. Effects of the Environment on Nonadiabatic Processes

It is often the case that nonadiabatic processes occur not in the gas phase but in complex environments, including solutions and biological environments such as proteins. The environment exerts its effect on nonadiabatic processes in several ways. One obvious interaction is energy dissipation, that is, the irreversible transfer of energy from the system to the environment. A second type of interaction is more subtle, reflecting differential interactions of the distinct electronic states with the environment. This can serve to move or even remove conical intersections between the potential energy surfaces in question.

The partitioning of the Hamiltonian into bath or environment and system modes can be accomplished in many ways. A first-principles approach to this partitioning has been introduced by Gindensperger, Burghardt, and Cederbaum,[127,128] denoted *GBC*1 and *GBC*2, respectively, below. They observe that ultrafast dynamics induced by conical intersections is intrinsically quantum mechanical in nature and that while powerful quantum dynamical techniques such as the multiconfiguration time-dependent Hartree (MCTDH) method[103,129] can handle a considerable number of degrees of freedom—about 20−30, in conical intersection situations—quantum dynamical descriptions of general multimode systems is not feasible.

*GBC*1 developed an approximate strategy that allows for the treatment of the dynamics in high-dimensional conical intersection situations, possibly including the effects of dissipation. They describe a time-scale based, three-tier partitioning. A system−environment partitioning in introduced, where the "system" part corresponds to a subset of dominant modes, in conjunction with a transformation of the environmental modes to (few) effective modes, which accurately account for the short-time dynamics at the conical intersection. The effective modes couple, in turn, to a residual environmental Hamiltonian—comprising potentially very many modes—which influences the dynamics on intermediate

dx.doi.org/10.1021/cr2001299 |*Chem. Rev.* 2012, 112, 481–498

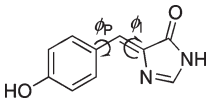

Figure 4. HBI, *p*-hydroxybenzylidene imidazolinone, a model chromophore for GFP. Isomerization described in terms of ϕ_p and ϕ_I. See text. Reprinted with permission from ref 133. Copyright 2009 American Chemical Society.

and long time scales. The impact of the (many) environmental modes on the system is thus recast in terms of a primary interaction between the system and the effective environmental modes, and a secondary process by which the effective modes couple to the "residual environment". The presented work proposes, for the first time, a dynamical description in terms of effective modes in a general conical intersection situation. In particular, it is shown that exactly *three* effective modes are required in the general case in the short-time limit.

GBC2 provide rules to estimate the quality of the effective-mode formulation described above for true macrosystems. A key parameter is the effective-mode period. Artificial recurrences, due to the neglect of the rest of the environment, are expected to occur at these periods. Regarding the autocorrelation functions, the results given by this approach are thus expected to be good up to the first artificial recurrence, i.e., up to about the value of the smallest of the effective-mode periods. This tendency is general. However, due to the interaction of the effective modes with the modes of the system via the conical intersection, the artificial recurrences may be altered and sometimes even suppressed.

Another promising approach to this problem exploits hybrid quantum mechanical (QM), molecular mechanical (MM), and QM/MM methods, developed for excited states by Warshel and Levitt[130] and subsequently by others.[131,132] In this approach, the total system is partitioned into a part that is treated quantum mechanically, the system, and a part that is treated by molecular mechanics, the environment. The electronic Hamiltonian is partitioned as[133]

$$H^e \approx H^{QM} + H^{MM} + H^{QM/MM}$$

where H^{QM} is the exact (Coulomb approximation) Hamiltonian for the system, H^{MM} is the molecular mechanics force field, and $H^{QM/MM}$ describes the interaction. The most problematic part of this decomposition is the $H^{QM/MM}$ part, particularly when there exist covalent bonds between the QM and MM regions. This "link atom" problem, which is particularly challenging when ground and excited states exist, has been addressed using the multicentered valence electron effective potential (MC-VEEP) method.[134]

Martínez and co-workers[133] have used this approach to report QM/MM simulations of the spectra and excited-state dynamics of biologically relevant chromophores including green fluorescent protein (GFP), photoactive yellow protein (PYP), and retinal protonated Schiff base (RPSB). Here we briefly review the GFP work, which is representative.

A model GFP chromophore *p*-hydroxybenzylidene imidazolinone (HBI), pictured in Figure 4, was used. In the protein environment GFP fluoresces, but in alternative environments, solution or gas phase, the fluorescence is quenched. As seen when comparing the gas-phase and solution-phase results, quenching is much slower in the gas phase than in solution. The two torsional angles pictured in Figure 4 are key.

Note that conjugated π-systems are a recurring theme in biosystems. The fluorescence is initiated by an electronic excitation of the $\pi-\pi^*$ type, which enables twisting about ϕ_I or ϕ_p. This twisting leads to the region of an S_1/S_0 conical intersection where quenching can occur. Martínez and co-workers observe that at least three explanations are possible for the different behaviors observed in the gas phase, solution, and protein: (i) different S_1 dynamics resulting in dramatically different arrival times at the conical intersection seam; (ii) differences in the accessibility of the conical intersection; and finally (iii) differences in the local topography of the conical intersection, that is, differences in the $\mathbf{s}^{I,J}$, $\mathbf{g}^{I,J}$, and $\mathbf{h}^{I,J}$ parameters. They show that the correct answer is (ii). In the gas phase, the minimum energy conical intersection lies above a minimum on S_1, creating a local barrier to reaching the conical intersection. The interaction with the solvent changes this topography, making the S_1/S_0 conical intersection the lowest energy point on the S_1 potential energy surface in this region. These studies were carried out at the CAS(2,2)/6-31G level of electronic structure theory, which was shown to mimic higher-level treatments of the electronic structure, thereby permitting treatment of the nuclear motion using AIMS.

Turning now to the protein environment, here the full GFP chromophore was modeled in a protein environment, using QM/MM techniques, based on a semiempirical configuration interaction wave function. The gas-phase calculations showed that quenching of S_1 depends on torsional motion that allows the system to reach the S_1/S_0 conical intersection seam. Thus, it is not surprising that dynamics simulations of the full GFP chromophore in a protein environment find relatively small changes in ϕ_I or ϕ_p over at least several picoseconds, compared to twisting on the subpicosecond time scale observed in solution.

2.6. Control of Nonadiabatic Chemical Dynamics with Lasers

2.6.1. Routing and the Branching Plane. Conical intersections represent points at the intersection of potential energy surfaces where access to distinct breakup channels is possible. The resulting influence of conical intersections on nuclear dynamics is referred to as routing. This is illustrated in Figure 5 for the reaction of OH with H_2. There it is seen how motion along modes defining the branching plane can lead to distinct outcomes. Motion along +**g** pushes the OH and H_2 molecules apart and at the same time decreases both r(HH) and r(OH) bond lengths; therefore, it is reasonable to assume that the OH−H_2 complex will continue to move apart and dissociate to OH−H_2, as is indeed found to be the case for representative gradient-directed paths.[135] Likewise, displacement along −**g** has the exact opposite effect. The OH and H_2 groups move closer together and their respective bond lengths grow slightly. It follows that such motion could be the start of a path leading to H_2O + H, as is confirmed when gradient-directed paths are followed.[135]

The ability of the branching plane to influence molecular motion makes nonadiabatic systems exhibiting conical intersections ideal candidates for laser control of chemical reactions.[136] Below we describe how this idea has been used.

2.6.2. Controlling Photoisomerization. Domcke and co-workers[137] used optimal control techniques to manipulate a model describing cis−trans photoisomerization of retinal in rhodopsin including a conical intersection. Coherent control mechanisms, in which laser pulses work cooperatively with a conical intersection, were studied. The authors carefully considered the relation between conical intersection topography and

dx.doi.org/10.1021/cr2001299 |*Chem. Rev.* 2012, 112, 481–498

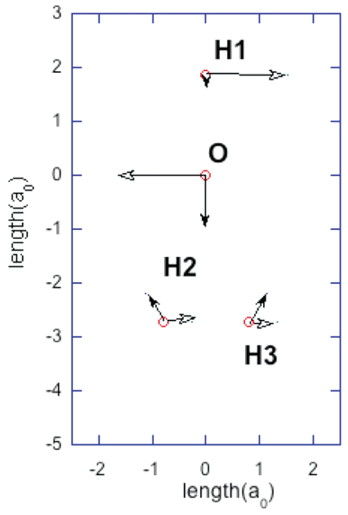

Figure 5. g−h plane for C_{2v} conical intersection in reaction of OH(A) with H_2; **g** vector solid arrows and **h** vector unfilled arrows.
Reprinted with permission from ref 135. Copyright 2000 American Institute of Physics.

pulse shaping. Optimally designed pulses largely consist of shaping subpulses, optimal pulses followed by an excitation subpulse that prepare a wave packet, which is localized along a reaction coordinate and has little energy in the coupling mode, $\mathbf{h}^{IJ}$. This shaping process achieves a high target yield. A related study was carried out by Flores and Batista.[138] These authors achieved control over product yields at finite time after photoexcitation by externally changing the relative *phases* of the photoexcitation pulses and consequently affecting the interference phenomena between individual wave packet components. Extensive coherent control over transient populations was predicted, despite the ultrafast decoherence phenomena induced by the electronic nonadiabaticity.

2.6.3. Cyclohexadiene (CHD)−Hexatriene (HT) Photoisomerization. The cyclohexadiene (CHD)−hexatriene (HT) photoisomerization is a much studied system.[139] Important theoretical work on this system has been done by Hofmann and de Vivie-Riedle.[140,141] Here we excerpt the work of Nakamura's group. It is observed experimentally that, when cyclohexadiene (CHD) is photoisomerized (in solution) producing both CHD and hexatriene (HT), the CHD/HT ratio is ∼6:4.[142] Nakamura has suggested that laser manipulation of the branching plane dynamics can be exploited to achieve control of, that is, alter, this measured branching ratio. Nakamura and co-workers studied manipulation of the cyclohexadiene (CHD)−hexatriene (HT) photoisomerization computationally.[143−145] The process to be manipulated can be summarized as follows: an initial wave packet is excited from S_0 to S_1 near the equilibrium geometry of CHD. After evolving on S_1, the wave packet encounters an S_0−S_1 conical intersection in the vicinity of a five-membered ring structure, pictured in Figure 6B. The two coordinates used to describe the branching plane for this conical intersection (R, θ) are shown in Figure 6A.

In this region the wave packet bifurcates into paths leading to both ground-state CHD and HT. Nakamura's manipulation of his computational simulation of the branching ratio is accomplished as follows: an initial wave packet with *directed momentum* pointing toward the five-membered ring conical intersection is (i) prepared in the ground state of CHD and (ii) efficiently

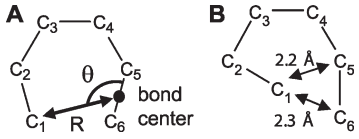

Figure 6. (A) Two-dimensional Jacobi coordinates used in the wave packet dynamics. (B) Schematic molecular geometry at the five-membered ring S_1−S_0 conical intersection minimum (the minimum on the conical intersection hypersurface).
Reprinted with permission from ref 145. Copyright 2010 American Chemical Society.

excited to S_1 using a quadratically chirped pulse. The directed wave packet moves directly from the Franck−Condon region on S_1 to the five-membered ring conical intersection, avoiding other regions sampled by an unoriented initial wave packet. The directed wave packet produces mostly HT on S_0 after passing through the conical intersection. This is in contrast to the ∼50:50 mixture produced by a simulation of the unoriented wave packet. This 50:50 CHD/HT branching ratio is in good accord with the ∼60:40 measured ratio and serves to lend credibility to the computational analysis.

2.6.4. Vibrationally Mediated Photodissociation of NH_3. We now turn to a related problem where the computational analysis is less satisfactory at present. Vibrationally mediated photodissociation provides an experimental means to manipulate the outcome of nonadiabatic photodissociation involving conical intersections. The initial vibrational level, **n**, of a molecule prior to photodissociation can affect the outcome of the dissociation as measured by the branching fractions. A particularly dramatic example of this is the photodissociation of NH_3,

$$NH_3(\tilde{X}^1A_1, \mathbf{n}) + h\nu \rightarrow NH_3(\tilde{A}) \rightarrow NH_2(\tilde{X}, \tilde{A}) + H \quad (17)$$

described in a now classic series of papers by Crim's group.[146−148] Crim determined that photodissociation of NH_3 with an excited N−H symmetric stretch produces primarily ground-state NH_2 along with a H atom. However, the situation was very different for electronically excited molecules containing a quantum of antisymmetric N−H stretch. Decomposition from that state produces almost exclusively electronically excited $NH_2(\tilde{A})$.

Truhlar and co-workers have addressed the question of mode specificity in reaction 17.[110] It is dfficult to use direct dynamics address this question. In direct dynamics the electronic structure data, energies, energy gradients, and derivative couplings are provided "on demand" when called for by the (time-dependent) dynamics simulation. The "on-demand" incorporation of ab initio data makes the use of state of the art electronic structure methods impractical. To circumvent the accuracy issue, Truhlar and co-workers[73,149] developed a sophisticated coupled diabatic state representation of the $1,2^1A$ states of NH_3 based on the 4-fold way diabatization scheme.[85] They then used those coupled potential energy surfaces with several quasi-classical trajectory dynamics schemes to simulate reaction 17.[110] Their work provided a deep understanding of the nonadiabatic dynamics and issues that must be addressed when simulating the experiment. They conclude that it was disappointing that their calculations do not reproduce the experimental mode specificity at the experimental energies. They observe that further work is required to determine the origin of the discrepancy. More recently

dx.doi.org/10.1021/cr2001299 |*Chem. Rev.* 2012, 112, 481–498

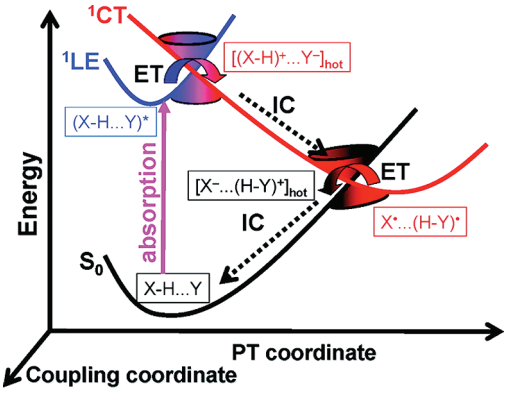

Figure 7. Schematic view of the electron-driven proton transfer (EDPT) process in intermolecularly hydrogen-bonded systems. Abbreviations: LE, locally excited state; CT, charge-transfer state; ET, electron transfer; IC, internal conversion. The colors indicate schematically the mixing of the electronic wave functions at the conical intersections. Reprinted with permission from ref 152. Copyright 2007 American Chemical Society.

a fully quantum mechanical dynamics treatment, based on the $\mathbf{H}^d$ obtained by Truhlar's group,[73,149] has also failed to reproduce the observed mode specificity.[150]

2.6.5. Controlling Radiationless Decay. Another instance of using lasers to control radiationless decay is provided by Christopher, Shapiro, and Brumer.[151] They use quantum interference induced by laser excitation to manipulate radiationless decay in a model pyrazine system. By preparing a linear combination of zeroth-order states on one Born−Oppenheimer surface, quantum interference can either maximize or minimize the population that undergoes a radiationless transition at a preset target time. Phase control is achieved by the presence of overlapping resonances. Significantly, conical intersections were not explicitly exploited in this analysis.

2.7. Conical Intersections and Mechanism for Nonadiabatic Reactions in Photobiology

As we have seen in previous sections in this review, nonadiabaticity is a recurring theme in biological systems. From the perhaps myopic perspective of this review, this reflects nature's effective use of conical intersections to harness energetic photons in general and sunlight in particular.

2.7.1. Electron-Driven Proton Transfer. As observed previously in the work of Martínez and co-workers,[133] conical intersections play a key role in quenching fluorescence in biologically relevant molecules. Sobolewski and Domcke[152] have emphasized the general importance of electron-driven proton-transfer (EDPT) processes in the functioning of hydrogen-bonded biologically relevant systems including organic photostabilizers. Fluorescence quenching in protic solvents, and the photostability of biological molecules, are also related to EDPT processes. Sobolewski and Domcke construct a mechanistic paradigm for the EDPT reaction. The paradigm is summarized in Figure 7, taken from ref 152 and elucidated here.

In the first step of EDPT, absorption takes ground-state X−H···Y to excited (X−H···Y)*, typically a $^1\pi\pi^*$ state. This is followed by an avoided crossing with a charge-transfer state of $^1\pi\sigma^*$ character (although $^1\pi\pi^*$ may be charge transfer), resulting in a highly polar excited state. The proton follows the electron stabilizing the biradical, producing X*···(H−Y)*. Back transfer of the electron at the S_1-S_0 conical intersections results in rapid internal conversion, producing $X^-\cdots(H-Y)^+$, which then decays to the original ground state X−H···Y. This motif was deduced from elaborate electronic structure calculations of (i) hydrogen transfer of photoacids to hydrogen-accepting solvents, (ii) photobases in a hydrogen-donating solvent environment, (iii) fluorescence quenching via hydrogen bonds, and finally (iv) intramolecularly hydrogen-bonded π-systems, which revealed the mechanism of excited-state intramolecular proton transfer (ESIPT) as explained in ref 152.

2.7.2. Intersection Space, Reaction Mechanisms, and Nonadiabatic Dynamics. It was noted in section 1 that points of conical intersection are not isolated but are continuously connected, forming the intersection or seam space. Robb and co-workers have identified the relation between nuclear motion and the locus of the seam space as key to understanding the mechanism of nonadiabatic processes.[47,50] They have studied the dynamics using surface hopping and more advanced quantum dynamics techniques based on the MCTDH approach.[106,107] Robb and co-workers emphasize two key points: (i) the relevant points in the intersection space are those where the reaction path meets the seam, and this need not be at the minimum of the seam; and (ii) radiationless decay takes place in the branching plane as one passes through the conical intersection.

As an example of this, Robb cites[153,154] the reversible protein photoreceptor, photoactive yellow protein (PYP), mentioned previously in this review. This protein consists of a chromophore *p*-coumaric acid, again a π-conjugated system, bound to a protein. The key step is a photoinduced cis−trans isomerization. Cis−trans isomerizations involving conical intersections are also a recurring theme in this review. Robb and co-workers compare the isolated chromophore with the chromophore in the protein environment. PYP provides a dramatic example of a situation where the reaction path is perpendicular to the branching plane coordinates. The chromophore both in vacuum and in the protein exhibits an extended seam along the cis−trans isomerization coordinate. Skeletal motions constitute the branching plane. In vacuo motion along the cis−trans isomerization coordinate encounters a minimum and a transition state before encountering a second minimum at the half twist. In the protein the S_1 potential energy surface is stabilized so that the conical intersection seam intersects the reaction path. Nuclear dynamics calculations serve to quantify these differences. In the isolated chromophore, the system never makes it to the conical intersection where quenching occurs. In the protein environment, the quenching fraction of trajectories was ~0.3, close to the experimental quantum yield of 0.35. In the interest of full disclosure, we note that Martínez and co-workers[155] have demonstrated the importance of the electrostatic environment in determining the outcome of photoexcitation in PYP.

2.8. Nonadiabatic Photoelectron Spectroscopy

Photoelectron spectroscopy and its time-resolved form are powerful tools for quantifying molecular electronic structure and molecular dynamics including both adiabatic energy transfer and nonadiabatic energy transfer including intersystem crossing and internal conversion. This is demonstrated in the plethora of review articles that have appeared in recent years.[156−163] Although this review focuses on time-independent computations, time-resolved simulations for states coupled by conical intersections have been reported.[164] In photoelectron spectroscopy an electron is photodetached (photoionized) from an anion (neutral) producing a neutral

dx.doi.org/10.1021/cr2001299 |*Chem. Rev.* 2012, 112, 481–498

(positive ion), the residual molecule. The electrons are collected, and the resulting spectrum is that of the residual molecule. Below we will use the language of anion-photodetachment spectroscopy, although the results are equally applicable to photoionization. The effect of the spin−orbit interaction is considered when appropriate.

2.8.1. General Formulation—Vibronic Coupling Model. In the vibronic coupling model, the wave function for the photodetached species is given by eq 5b,

$$\Psi_K^T(\mathbf{q}^N,\mathbf{w}) = \sum_{I=1}^{N^{\text{state}}} \Psi_I^d(\mathbf{q}^N;\mathbf{w})\zeta_I^K(\mathbf{w}) \tag{18a}$$

where we use $\mathbf{w}$ to denote N^{int} internal coordinates and $\mathbf{q}^N = (\mathbf{q}_1, \mathbf{q}_2, ..., \mathbf{q}_N)$ to denote the coordinates of the N electrons. The $\zeta_I^K(\mathbf{w})$ are in turn expanded in the multimode vibrational basis

$$\zeta_I^K(\mathbf{w}) = \sum_{\mathbf{m}} d_{I,\mathbf{m}}^K \Theta_{\mathbf{m}}^{(n)}(\mathbf{w}) \tag{18b}$$

where the $\Theta_{\mathbf{m}}^{(n)}(\mathbf{w})$ are expressed as multimode products

$$\Theta_{\mathbf{m}}^{(n)}(\mathbf{w}) = \prod_{j=1}^{N^{\text{int}}} \chi_{m_j}^{(n),j}(w_j) \tag{18c}$$

Here $0 \le m_j < M_j$ and $\chi_m^{(n),j}$ is the mth harmonic oscillator function associated with the jth mode. Using $\mathbf{H}^d$ determined as in section 2.2, the nonrelativistic vibronic Schrödinger equation, eq 5a, becomes

$$\sum_{k,\mathbf{n}} H_{\mathbf{m},\mathbf{n}}^{l,k} d_{k,\mathbf{n}}^K = E_K^T d_{l,\mathbf{m}}^K \tag{19a}$$

where $1 \le k, l \le N^{\text{state}}$ and

$$H_{\mathbf{m},\mathbf{n}}^{k,l} = \langle \Theta_{\mathbf{m}}^{(n)}(\mathbf{w}) | T^{\text{nuc}}\delta_{k,l} + H_{k,l}^d(\mathbf{w}) | \Theta_{\mathbf{n}}^{(n)}(\mathbf{w}) \rangle \tag{19b}$$

$H_{\mathbf{m},\mathbf{n}}^{k,l}$ is an N^T by N^T matrix, where

$$N^T = N^{\text{state}} N^{\text{vib}} \tag{20a}$$

in which

$$N^{\text{vib}} = \prod_{i=1}^{N^{\text{int}}} M_i \tag{20b}$$

From the form of $\mathbf{H}^d$ for bound states, eq 13, the matrix elements of $H_{\mathbf{m},\mathbf{n}}^{k,l}$ are easily evaluated.[79] However, although the nonzero elements of $H_{\mathbf{m},\mathbf{n}}^{k,l}$ grow only linearly[165] with N^{vib}, from eq 20b, N^{vib} grows rapidly with N^{int}. To deal with the large dimension of $H_{\mathbf{m},\mathbf{n}}^{k,l}$, Schuurman, Yarkony, and co-workers developed an open-ended, fine-grained, parallel, Lanczos-based algorithm to determine the coupled vibronic wave functions.[101,165] The open-ended, fine-grained, parallel design of the algorithm not only dramatically reduces the time to solution for the nonadiabatic wave function but also permits basis set expansions currently on the order of 10 billion terms, 100 times the size that can be treated using conventional, single-processor methods.[165]

The wave function for the anion with total energy E_α^T has the following form:

$$\Psi_\alpha^{T,an}(\mathbf{q}^{N+1},\bar{\mathbf{w}}) = \Psi_0^{a(an)}(\mathbf{q}^{N+1},\bar{\mathbf{w}})\Theta_{\boldsymbol{a}}^{(an)}(\bar{\mathbf{w}}) \tag{21a}$$

where $\Psi_0^{a(an)}$ is the ground electronic state of the anion, $\bar{\mathbf{w}} = \bar{\mathbf{T}}(\mathbf{Q} - \mathbf{Q}^{0,(an)})$, $\mathbf{Q}$ denotes a set of N^{int} internal coordinates,

$$\Theta_{\boldsymbol{a}}^{(an)}(\bar{\mathbf{w}}) = \prod_{j=1}^{N^{\text{int}}} \chi_{a_j}^{(an),j}(\bar{w}_j) \tag{21b}$$

$\Theta_{\boldsymbol{a}}^{(an)}(\bar{\mathbf{w}})$ is the vibrational wave function for the anion in its ground electronic state, and $\chi_m^{(an),j}$ is the mth harmonic oscillator function associated with the jth mode of the anion. Here $\mathbf{Q}^{0,(an)}$ is the ground-state equilibrium geometry of the anion and the $\bar{\mathbf{w}}$ are its normal coordinates, with the ground vibrational state denoted $\boldsymbol{a} = (0, 0, ..., 0) = \mathbf{0}$. We call attention to the fact the neutral coordinates ($\mathbf{w}$) and anion coordinates ($\bar{\mathbf{w}}$) need not be the same. This is the origin of the Duschinsky effect.[166,167] It is discussed further following eq 23c.

The spectral intensity distribution function, $I(E)$, is given by

$$I(E) = \sum_\alpha \rho(\alpha) \sum_K |A_{\alpha,K}|^2 \delta(E - (E_K^T - E_\alpha^T)) \tag{22a}$$

where ρ is the population of the anion state α and the amplitude, $A_{\alpha,K}$, is given by

$$A_{\alpha,K} = \langle \Psi_\alpha^{T,an}(\mathbf{q}^{N+1},\bar{\mathbf{w}}) | \mu | \Psi_K^T(\mathbf{q}^{N+1},\mathbf{w}) \rangle_{\mathbf{q}^{N+1},\mathbf{w}} \tag{22b}$$

Note that in eq 22b Ψ_K^T is an $N+1$ electron function rather than the N-electron function as in eq 18a. This reflects an approximate treatment of the electron-detachment process, the sudden approximation, in which the detached electron resides in an orbital that is orthogonal to the orbitals in the residual molecule and approaches a plane wave for large values of the electron coordinate. The residual molecule is unaltered by the inclusion of the orbital for the detached electron. Inserting eqs 18a and 21a into eq 22b gives

$$\begin{aligned} A_{\alpha,K} &= \sum_{I,\mathbf{m}} d_{I,\mathbf{m}}^K \langle \Theta_{\boldsymbol{a}}^{(a)}(\bar{\mathbf{w}}) | \mu_{I,K,\mathbf{k}}^0 | \Theta_{\mathbf{m}}^{(n)}(\mathbf{w}) \rangle_{\mathbf{w}} \\ &\approx \sum_{I,\mathbf{m}} d_{I,\mathbf{m}}^k f_{\mathbf{m}}^{\boldsymbol{a}} \mu_{I,K,\mathbf{k}}^0(\mathbf{w}^{FC}) \end{aligned} \tag{23a}$$

In eq 23a the Franck−Condon approximation has been used to derive the approximate equality and

$$\mu_{I,K,\mathbf{k}}^0(\mathbf{w}) = \langle \Psi_0^{a(an)}(\mathbf{q}^{N+1},\bar{\mathbf{w}}) | \mu^{N+1} | A^c \Psi_I^d(\mathbf{q}^N,\mathbf{w}) \phi_K^{\mathbf{k}}(\mathbf{q}_{N+1}) \rangle_{\mathbf{q}^{N+1}} \tag{23b}$$

$$\begin{aligned} f_{\mathbf{m}}^{\boldsymbol{a}} &= \langle \Theta_{\boldsymbol{a}}^{(an)}(\bar{\mathbf{w}}) | \Theta_{\mathbf{m}}^{(n)}(\mathbf{w}) \rangle \\ &= \langle \prod_{j=1}^{N^{\text{int}}} \chi_{a_j}^{(an),j}(\bar{w}_j) | \prod_{j=1}^{N^{\text{int}}} \chi_{m_j}^{(n),j}(w_j) \rangle \end{aligned} \tag{23c}$$

In eq 23b, $\mathbf{k}$ labels the momentum of the outgoing electron and the intersystem antisymmetrizer A^c insures that the ket, $A^c(\Psi_I^d(\mathbf{q}^N,\mathbf{w})\phi_K^{\mathbf{k}}(\mathbf{q}_{N+1}))$, is fully antisymmetric. The multidimensional Franck−Condon integrals, in eq 23c are evaluated using recursion relations[168−173] adapted to parallel processing.[174]

In adiabatic simulations, $\bar{\mathbf{w}}$ and $\mathbf{w}$ are the normal coordinates of anion and neutral, respectively. In this case, the Franck−Condon overlaps in eq 23c give directly the peak heights in a spectral simulation. In terms of $\mathbf{Q}$, these coordinate systems are in general shifted and rotated relative to each other, resulting in the Duschinsky rotation effect.

The determination of the electronic transition moment in eq 23b is a significant issue in photoelectron spectroscopy.[175−177] As noted above, eq 23b reflects the fact that the wave function for the residual molecule plus detached electron is written as an antisymmetrized product of the vibronic wave function for the Kth channel times a geometry-independent orbital $\phi_k^{\mathbf{k}}(\mathbf{q}_{N+1})$.

dx.doi.org/10.1021/cr2001299 |Chem. Rev. 2012, 112, 481–498

This is an approximation, and we have recently derived a more precise result.[178,179] This issue, which is properly the province of the electron-scattering community,[180−183] is discussed further below. However, it is possible to make significant progress with simple approximations for $\mu^0_{I,k,\mathbf{k}}$, as we show in sections 2.8.3 and 2.8.4.

2.8.2. Spin−Orbit Effects. When the spin−orbit interaction is included, the total Hamiltonian becomes

$$H^{T,so} = T^{\text{nuc}} + H^e + H^{so} \equiv H^T + H^{so} \tag{24}$$

where H^{so} is the spin−orbit interaction in the Breit−Pauli approximation.[184] The relativistic wave function satisfies

$$(H^{T,\text{so}} - E_M^{T,\text{so}})\Psi_M^{T,\text{so}}(\mathbf{q}^N, \mathbf{w}) = 0 \tag{25}$$

For molecules composed of atoms in the third period or earlier, the solutions of the relativistic Schrödinger equation can be expanded in terms of the eigenstates of the nonrelativistic Schrödinger equation. This approach has both conceptual and computational advantages. When heavier atoms are present, an alternative approach, based on a elegant analysis of the symmetry of H^{so}, which treats the spin−orbit and Coulomb contributions more equivalently, due to Poluyanov and Domcke is available.[185,186]

Instead of working in the standard M_s basis we use the time-reversal adapted basis introduced by Mead.[187] This basis simplifies the form of the matrix elements of H^{so}. For doublet states, which is the case we deal with, the basis is given by

$$-\Psi^{e,d}_{l,\pm}(\mathbf{q}^N, \mathbf{w}) = \pm(1/\sqrt{2})[\tilde{\Psi}^{e,d}_{l,1/2}(\mathbf{q}^N, \mathbf{w}) \pm i\tilde{\Psi}^{e,d}_{l,-1/2}(\mathbf{q}^N, \mathbf{w})] \tag{26}$$

where $\tilde{\Psi}^{e,d}_{l,M_s}$ is the diabatic wave function in eq 4a, in which we have explicitly included the M_s value. Then the relativistic wave function $\Psi^{T,so}_M$ is expanded as

$$\Psi_M^{T,\text{so}}(\mathbf{q}^N, \mathbf{w}) = \sum_{K,s} \rho^M_{K,s}\Psi^T_{K,s} \equiv \sum_{K,s,l,\mathbf{m}} \rho^M_{K,s}[d^K_{l,\mathbf{m}}\Psi^d_{l,s}(\mathbf{q}^N, \mathbf{w})\Theta^{(n)}_{\mathbf{m}}(\mathbf{w})] \tag{27}$$

where $s = \pm$ and the $\rho^M_{k,s}$ satisfy

$$\left(\begin{pmatrix} \mathbf{E}^{(nr)} & 0 \\ 0 & \mathbf{E}^{(nr)} \end{pmatrix} + \begin{pmatrix} \mathbf{H}^{so}_{+,+} & \mathbf{H}^{so}_{+,-} \\ \mathbf{H}^{so}_{-,+} & \mathbf{H}^{so}_{-,-} \end{pmatrix}\right)\begin{pmatrix} \rho^M_+ \\ \rho^M_- \end{pmatrix} = E^{T,so}_M \begin{pmatrix} \rho^M_+ \\ \rho^M_- \end{pmatrix} \tag{28}$$

with $E^{(nr)}_{I,J} = \delta_{I,J}E^T_J$ and $H^{so}_{I,s;J,s'} = \langle\Psi^T_{I,s}|H^{so}|\Psi^T_{J,s'}\rangle$ for $s,s' = \pm$. From the definition of $H^{so}_{I,s;J,s'}$, the spin−orbit interaction is seen to be, in a Franck−Condon-like approximation, a raw electronic matrix element *reduced* by a vibrational overlap term.[188] This reduction of the raw electronic matrix element is an example of the Ham reduction effect.[189]

From eq 27 we can show[188]

$$I^{(so)}(E) = \sum_M I^{(so)}_{M,\alpha}\delta(E - (E^{T,so}_M - E^T_\alpha)) \tag{29a}$$

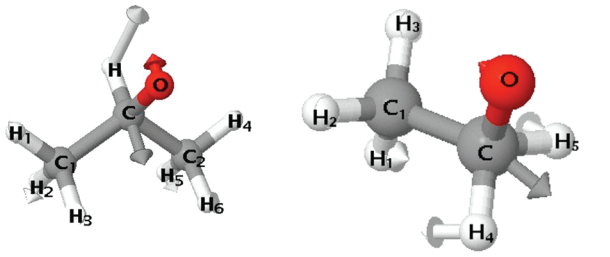

Figure 8. **g** for isopropoxy resembles that of methoxy. That for ethoxy does not.
g vector from isopropoxy is reprinted with permission from ref 99, and that from ethoxy is reprinted with permission from ref 100. Copyright 2009 American Institute of Physics.

where

$$2I^{(\text{so})}_{M,\alpha} = \left[\sum_K \rho^M_{K,+}A_{\alpha,K}\right]^2 + \left[\sum_K \rho^M_{K,-}A_{\alpha,K}\right]^2 \tag{29b}$$

which exhibits the promised intensity borrowing.

An example of the use of these computational tools to predict and explain measured spectra follows. This example also demonstrates the value of the $g-h$ plane in understanding conical intersections.

2.8.3. Photoelectron Spectra of Isopropoxide.[99] In this section a simulation of the photoelectron spectrum of isopropoxide, reported in ref 99 and denoted *DY*, is reviewed. The corresponding neutral molecule isopropoxy is a double, methyl for hydrogen, substitutional isomer of the well-studied Jahn−Teller molecule, methoxy, CH_3O, whose ^{2}E ground state is known to exhibit both a Jahn−Teller instability and the effects of the spin−orbit interaction.[190] Methyl substitution splits the ^{2}E state into a ^{2}A′ state and a ^{2}A″ state. Lineberger and co-workers, who measured the photoelectron spectrum of isopropoxide over a decade ago,[191] reported the splitting of these states, the $\tilde{A}-\tilde{X}$ separation, to be 1225 ± 65 cm^{-1} in isopropoxy. This assignment was based on absence of this line from an adiabatic simulation of the ground state and supported by the intuitive but, as we show later, incorrect assumption that the $\tilde{A}-\tilde{X}$ splitting in isopropoxy should be larger than that in ethoxy, because the former is more perturbed, compared to methoxy. Subsequently Miller and co-workers[192] determined, from dispersed fluorescence experiments, the $\tilde{A}-\tilde{X}$ separation in isopropoxy to be only 68 ± 10 cm^{-1}. In an unpublished slow electron velocity-map imaging (SEVI) result, Neumark[193] also found a similarly positioned transition at 68 cm^{-1} in isopropoxy, consistent with Miller's result.

Using the algorithms described in sections 2.8.1 and 2.8.2, *DY* were able to understand and explain these discrepancies. In this case, the ability to include the spin−orbit interaction was essential, as was the ability to describe a conical intersection in terms in terms of unique **g** and **h** vectors. The explanation for the above observations is as follows. Not surprisingly, single adiabatic state representations of the electronic states are poor predictors of these spectra.

*(i). **g**−**h** Plane Analysis.* *DY* showed that, perhaps counterintuitively, isopropoxy is actually close to the parent methoxy. This was determined by comparing the **g** and **h** vectors for isopropoxy with those of methoxy. The **g** vectors illustrate the situation. In methoxy the **g** vector is principally a ∠OCH bend. As Figure 8 illustrates, this is also the case in isopropoxy but not,

dx.doi.org/10.1021/cr2001299 |*Chem. Rev.* 2012, 112, 481–498

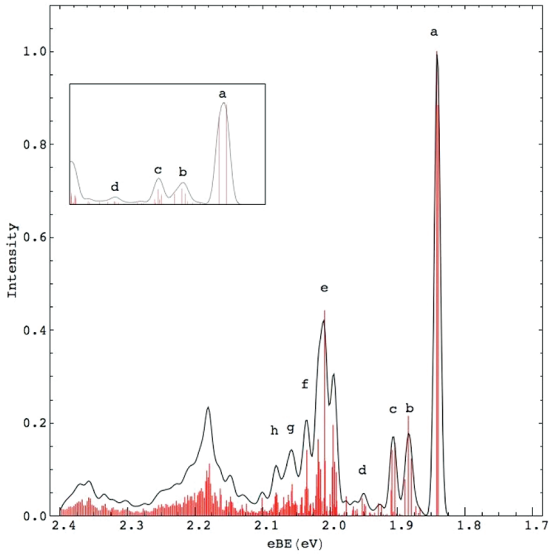

Figure 9. Photoelectron spectrum of isopropoxy, which is in good agreement with the measured spectrum (not shown). Inset is the low-energy computed spectrum including spin−orbit interaction with the resolution of 100 cm^{-1} resolution. The two lines under the peak labeled *a* in the inset, resolved in dispersed fluorescence experiments,[192] give the computed 61.9 cm^{-1} $\tilde{A}-\tilde{X}$ splitting. Peak *a* could not be resolved in an earlier photoelectron experiment.[191]
Reprinted with permission from ref 99. Copyright 2009 American Institute of Physics.

for example, in the less substituted ethoxy, where the **g** vector is a more complicated bend.[100]

Further in isopropoxy, $||\mathbf{g}|| \approx ||\mathbf{h}||$, as it is exactly in methoxy. Thus, it is not surprising that isopropoxy behaves approximately like a C_{3v} molecule. This observation holds the key to understanding the discrepancies in the $\tilde{A}-\tilde{X}$splitting in isopropoxy.

(ii). Nonrelativistic Energy Splittings. In methoxy the splitting of the two lowest lines in the *nonrelativistic* vibronic spectrum, the nominal $\tilde{A}-\tilde{X}$ splitting, is 0 by symmetry. Therefore, it is not surprising that the separation of the two lowest lines in the nonrelativistic isopropoxy spectrum, the nominal $\tilde{A}-\tilde{X}$ splitting, is calculated to be only 17 cm^{-1}.[99]

(iii). Splittings Including the Spin−Orbit Interaction. Turning on the spin−orbit interaction resolved the remaining discrepancy. First, we provide some background. The $X^2\Pi$ state of OH is the analogue of the $\tilde{X}^2$E state in methoxy. In OH the spin−orbit induced splitting is ∼126 cm^{-1}.[194] A similar splitting might be expected in methoxy, but in fact the measured spin−orbit splitting is closer to half that, being reported as 61.8,[195] 64,[196] and 63[197] cm^{-1}. The reduction of the size of the spin−orbit interaction is due to the Jahn−Teller effect and is known as Ham reduction.[189] When the spin−orbit interaction is included in isoproxy, the splitting of the lowest two states, the nominal $\tilde{A}-\tilde{X}$ splitting, increases from 17 to 61.9 cm^{-1}, now in good agreement with the measured value of ∼68 cm^{-1}. Thus, the 68 cm^{-1} splitting in isopropoxy is better thought of as the analogue of spin−orbit induced splitting in methoxy, rather than an $\tilde{A}-\tilde{X}$ splitting. Even the Ham reduction is similar. This splitting of 68 cm^{-1} in isopropoxy is too small to have been resolved in Lineberger's photoelectron spectrum, and because no asymmetry in the broadened line is predicted, the misassignment is explained (see Figure 9).

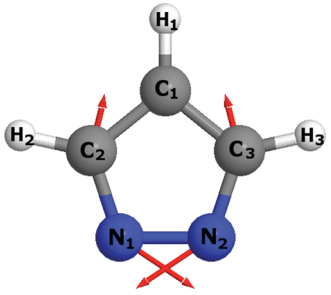

Figure 10. Pyrazolyl at its minimum energy conical intersection. **g** vector is indicated by arrows.
Reprinted with permission from ref 202. Copyright 2008 American Institute of Physics.

2.8.4. Azolyls—Remarkable Five-Membered Rings. The azolyls are five-membered nitrogen-containing heterocycles with the form $(CH)_xN_y$ with $x + y = 5$. They can be viewed as substitutional isomers of the cyclopentadienyl radical $(CH)_5$. The cyclopentadienyl radical, with D_{5h} symmetry, has a $^2E_1$" ground state.[198−200] This state, which is Jahn−Teller distorted, arises from a degenerate pair of π-orbitals, which are singly occupied. As a result of the Jahn−Teller distortion, the $^2E_1$" states splits into a $^2B_1$ and a $^2A_2$ state. Dillon et al.,[101] in a work denoted *DYS*1, refer to this situation as the cyclopentadienyl paradigm and observe that it holds for the monosubstituted radical $(CH)_4N$ pyrrolyl and the two $(CH)_3N_2$ radicals, imidazolyl and parazolyl. The paradigm fails for 1,2,3-triazolyl as explained by *DYS*1. The changes in the electronic properties of the azolyls with increasing numbers of nitrogens reflects the existence of a lone pair on nitrogen replacing the C−H σ-bond. It is much easier to excite an electron from a nitrogen lone pair than from a C−H σ-bond. As a result, as the number of proximal nitrogens increases the number of the low-lying states increases and their character changes. For 1,2,3-triazolyl, states arising from $n \rightarrow \pi$, excitations of $^2A_1$, and $^2B_1$ symmetry, where n is a nitrogen lone pair, need to be considered. Further Matsika and Yarkony[201] found that pyrazolyl, pictured in Figure 10, has a seam of three state conical intersections within ∼3400 cm^{-1} of the ground state, a result subsequently confirmed by Schuurman and Yarkony[202] and also by Stanton and co-workers.[79]

The low-lying excited states and three state intersections have a profound effect on the simulations of photoelectron spectra in the azolyls. Although the photoelectron spectrum of pyrrolyl can be well described by two electronic states,[203,204] the pyrazolyl simulation required three electronic states[79] and 1,2,3-triazolyl required that four states[101] be included.

The analysis of Lineberger, Stanton, and co-workers[79] of the pyrrazolyl photoelectron spectrum, denoted *LS*, using the nonrelativistic time-independent methodology outlined in section 2.8.1, is particularly compelling. Key results of that study are summarized in parts a and b of Figure 11, taken from *LS*. Figure 11a shows the simulation of the photoelectron spectrum of deuterated pyrazolide, pyrazolide-d_3, obtained with only the first two states included in the simulation. The agreement is seen to be less than good. However, when the three lowest states are included, Figure 11b agreement improves significantly.

It is significant to observe here that in the three state simulation the transition moment for the $^2A_2$ state was scaled by 0.92, to get the experimentally observed peak heights. For this

dx.doi.org/10.1021/cr2001299 |*Chem. Rev.* 2012, 112, 481–498

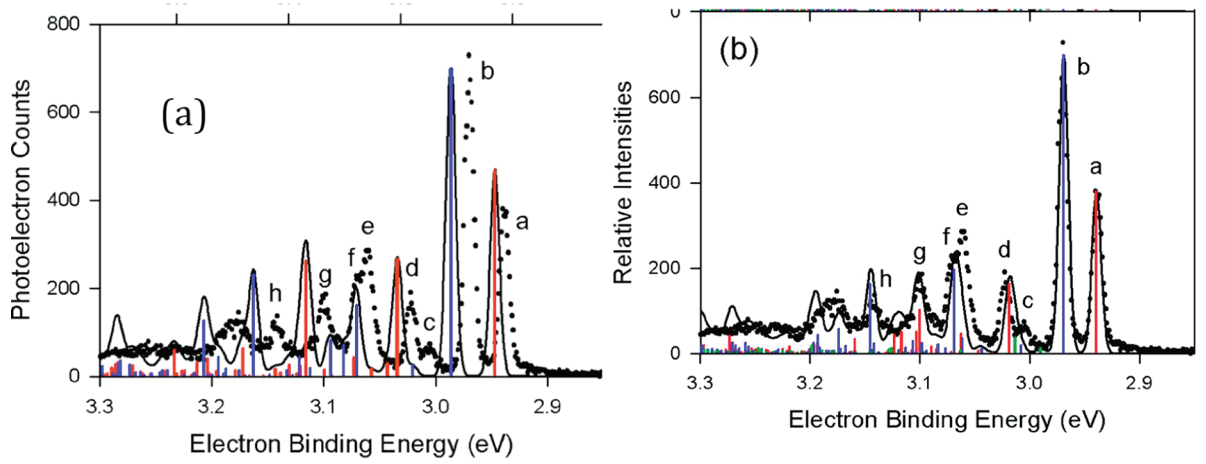

Figure 11. Photoelectron spectrum of pyrazolide revealing the spectrum of pyrazolyl. (a) A nonadiabatic simulation that includes the X^2A_2 and A^2B_1 states of the 1-pyrazolyl-d_3 radical, superimposed on the experimental spectrum (dots). The solid line is the simulated spectrum with a Gaussian convolution of a 10 meV full width at half-maximum. (b) A nonadiabatic simulation that includes the $X\ ^2A_2$, A^2B_1, and $B\ ^2B_2$ states of the 1-pyrazolyl-d_3 radical, which are fully coupled. The simulated spectrum is superimposed on the experimental spectrum (dots). The magnitude of the transition dipole moment for the X^2A_2 state has been scaled down by a factor of 0.92 in this simulation to match the relative intensities of the origin peaks for the $X\ ^2A_2$ and A^2B_1 states to those observed experimentally.
Reprinted with permission from ref 79. Copyright 2006 American Institute of Physics.

issue to be addressed from first principles, the electronic transition moments in eq 23b must be computed. This point is discussed further in section 3.

3. THE FUTURE

Several aspects of nonadiabatic processes will serve to keep their study in the forefront of chemistry. Nonadiabatic processes are at the center of any approach to efficiently harvest solar energy. Biological systems have developed elegant chromophore/protein systems for harvesting and utilizing visible and higher-energy photons. Thus, studies related to photocatalysis and solar energy production will remain of both fundamental and practical concern. More precise methods of treating these process are likely to emerge. For systems treated by multireference configuration interaction methods, interexcited state derivative couplings are correctly and efficiently evaluated using modern analytic gradient technology.[45,53] However, computational cost limits the systems for which this approach is applicable. For larger systems, density functional theory is frequently the method of choice. In this case, interexcited state derivative couplings are approximated. The accuracy and potential limitations of these approximations require additional study.

Improved treatments of nonadiabatic dynamics are needed. Mixed quantum-classical dynamics (MQCD) have enabled larger systems, i.e., more degrees of freedom, to be treated. However, all MCQD methods have intrinsic limitations in that they do not properly describe tunneling or zero point energy effects. Consequently, semiclassical methods may provide a path forward. Techniques to include the effects on the environment will continue to improve. Here it is important to note that methods that self-consistently adapt the environment to the system, the part treated by exact quantum mechanical dynamics, encounter difficulties when describing nonadiabatic processes, because more than one system state is involved. The partitioning techniques introduced by Burghardt, Cederbaum, and co-workers provide an interesting alternative. As far as current molecular mechanics treatments of the environment are concerned, perhaps the weak (least strong) link in the QM/MM simulation is the $H^{QM/MM}$ Hamiltonian, that portion of the Hamiltonian that describes the system−environment interactions. It can be expected that in the near future this aspect of the QM/MM simulation will be an active area of research.

In a related vein, Tully and co-workers observe[117] several directions in which work is needed to provide a unified theory of the interaction of molecules with metal surfaces. First electronic structure methods capable of determining the electronic states and their nonadiabatic interactions are needed. Tully cites progress using embedding techniques[205] but asserts that further advances are needed. In addition, concerning the desirability of fully quantum dynamics techniques, the need to treat motion of the metal surface only increases the demands on fully quantum methods.

Photobiology will continue to drive and benefit from technological advances. Mechanistic insights into these processes can be obtained from reliable electronic structure calculations. However, these studies should be augmented with treatments of the nuclear dynamics to address mechanistic issues, as in the furan study presented in section 2.1 or the intersection space analysis of Robb and co-workers in section 2.7.2. Nuclear dynamics studies will also address issues related to barrier tunneling, dynamics at conical intersections, and intramolecular vibrational relaxation (IVR). Such studies using surface-hopping methods and full quantum methods based on the fly AIMS and Gaussian-based MCDTH methods have already begun to appear.

As noted in section 2.8, great strides have been made in the simulation of photoelectron spectra using both time-dependent and time-independent methods. The advent of new slow electron detection schemes[163] and photoelectron imaging techniques[206−208] have increased the precision of the experimental measurements. Time resolved methods[162] have enabled new questions to be addressed. These increased capabilities present new challenges to nonadiabatic computation.

dx.doi.org/10.1021/cr2001299 |*Chem. Rev.* 2012, 112, 481–498

The electronic transition moment integral $\mu^0_{I,K,\mathbf{k}}$ in eq 23b in principle depends on both the diabatic electronic state $\Psi^d_I(\mathbf{q}^N, \mathbf{w})$ and the scattering orbital, $\phi^{\mathbf{k}}_K(\mathbf{q}_{N+1})$. The scattering orbital, in turn, depends on both the **k**-vector of the electron and the vibronic eigenstate (channel index) of the residual molecule.[178] It is common[5] to neglect the diabatic state, channel, and **k** dependence of $\mu^0_{I,K,\mathbf{k}}$ or to infer its diabatic state dependence from experimental measurements,[79,98] as in the pyrazoly example described in section 2.8.4. The computation of $\mu^0_{I,K,\mathbf{k}}$ is confounded by the fact that the Born−Oppenheimer approximation fails in the residual molecule and that low-energy electrons are produced. The correct determination of the relevant transition moment is an active area of research.[176−179] It is expected to be an important computational issue in the near future.

AUTHOR INFORMATION

Corresponding Author

*E-mail: yarkony@jhu.edu.

BIOGRAPHY

David R. Yarkony was born and grew up in New York City. He received his Bachelor's degree from the State University of New York at Stony Brook in 1971 and his Ph.D. from University of California at Berkeley, 1975, where his advisor was Henry F. Schaefer III. After two years as a postdoctoral research associate with Robert J. Silbey at the Massachusetts Institute of Technology, he joined the Department of Chemistry of the Johns Hopkins University, where he is today the D. Mead Johnson Professor of Chemistry. He is married to the former Kathryn McClelland of El Cerrito, CA, and has three children, Julian, Alexander, and Andrea (in order of appearance).

ACKNOWLEDGMENT

D.R.Y. wishes to thank Horst Köppel, John Tully, Todd Martínez, Hiroki Nakamura, Wolfgang Domcke, Joseph Dillon, Michael Schuurman, and John Stanton for permission to employ their figures in this work. D.R.Y. gratefully acknowledges the support of NSF grant CHE-1010644, which enabled preparation of this work. The cover art was provided by Joseph Dillon.

REFERENCES

(1) London, F. *Z. Phys.* **1932**, *74*, 132.
(2) *Quantum Chemistry. Classic Scientific Papers*; Hettema, H., Ed.; World Scientific: Singapore, 2000.
(3) Köppel, H.; Domcke, W.; Cederbaum, L. S. *Adv. Chem. Phys.* **1984**, *57*, 59.
(4) Yarkony, D. R. *Acc. Chem. Res.* **1998**, *31*, 511.
(5) Köppel, H.; Domcke, W.; Cederbaum, L. S. In *Conical Intersections*; Domcke, W., Yarkony, D. R., Köppel, H., Eds.; World Scientific: Hackensack, NJ, 2004; Vol. 15.
(6) Teller, E. *J. Phys. Chem.* **1937**, *41*, 109.
(7) Zener, C. *Proc. R. Soc. London A* **1932**, *137*, 696.
(8) Bardo, R. D.; Kleinman, L. I.; Raczkowski, A. W.; Wolfsberg, M. *J. Chem. Phys.* **1978**, *69*, 1106.
(9) Bardo, R. D.; Wolfsberg, M. *J. Chem. Phys.* **1977**, *67*, 593.
(10) Bardo, R. D.; Wolfsberg, M. *J. Chem. Phys.* **1978**, *68*, 2686.
(11) Kleinman, L. I.; Wolfsberg, M. *J. Chem. Phys.* **1974**, *60*, 4740.
(12) Kleinman, L. I.; Wolfsberg, M. *J. Chem. Phys.* **1974**, *60*, 4749.
(13) Bishop, D. M.; Cheung, L. M. *J. Chem. Phys.* **1983**, *78*, 1396.
(14) Bishop, D. M.; Cheung, L. M. *J. Chem. Phys.* **1984**, *80*, 4341.
(15) Handy, N. C.; Yamaguchi, Y.; Schaefer, H. F. *J. Chem. Phys.* **1986**, *84*, 4481.
(16) Jensen, J. O.; Yarkony, D. R. *J. Chem. Phys.* **1988**, *89*, 3853.
(17) Smith, F. T. *Phys. Rev.* **1969**, *179*, 111.
(18) Han, S.; Hettema, H.; Yarkony, D. R. *J. Chem. Phys.* **1995**, *102*, 1955.
(19) Baer, M. *Chem. Phys. Lett.* **1975**, *35*, 112.
(20) Baer, M. *Chem. Phys.* **1976**, *15*, 49.
(21) Baer, M. *Phys. Rep.* **2002**, *358*, 75.
(22) Mead, C. A.; Truhlar, D. G. *J. Chem. Phys.* **1982**, *77*, 6090.
(23) Cimiraglia, R.; Malrieu, J.-P.; Persico, M.; Spiegelmann, F. *J. Phys. B: At., Mol. Opt. Phys.* **1985**, *18*, 3073.
(24) Pacher, T.; Cederbaum, L. S.; Köppel, H. *J. Chem. Phys.* **1988**, *89*, 7367.
(25) Pacher, T.; Cederbaum, L. S.; Köppel, H. *Adv. Chem. Phys.* **1993**, *84*, 293.
(26) Pacher, T.; Mead, C. A.; Cederbaum, L. S.; Köppel, H. *J. Chem. Phys.* **1989**, *91*, 7057.
(27) Yarkony, D. R. *J. Chem. Phys.* **2000**, *112*, 2111.
(28) Köppel, H.; Gronki, J.; Mahapatra, S. *J. Chem. Phys.* **2001**, *115*, 2377.
(29) Yarkony, D. R. *J. Phys. Chem. A* **1998**, *102*, 8073.
(30) Ve'rtesi, T.; Vibók, Á.; Halász, a., G. J.; Baer, M. *J. Chem. Phys.* **2004**, *120*, 2565.
(31) Sadygov, R. G.; Yarkony, D. R. *J. Chem. Phys.* **1998**, *109*, 20.
(32) Abrol, R.; Kuppermann, A. *J. Chem. Phys.* **2002**, *116*, 1035.
(33) von Neumann, J.; Wigner, E. *Phys. Z.* **1929**, *30*, 467.
(34) Michl, J. *Top. Curr. Chem.* **1974**, 46.
(35) Bonacic-Koutecky, V.; Koutecky, J.; Michl, J. *Angew. Chem., Int. Ed. Engl.* **1987**, *26*, 170.
(36) Bonacic-Koutecky, V.; Schoffel, K.; Michl, J. *Theor. Chem. Acc.* **1987**, *72*, 459.
(37) Naqvi, K. R. *Chem. Phys. Lett.* **1972**, *15*, 634.
(38) Longuet-Higgins, H. C. *Proc. R. Soc. London A* **1975**, *344*, 147.
(39) Mead, C. A. *J. Chem. Phys.* **1979**, *70*, 2276.
(40) Klessinger, M.; Michl, J. *Excited states and the photochemistry of organic molecules*; VCH: New York, 1995.
(41) *Conical Intersections: Electronic Structure, Dynamics and Spectroscopy*; Domcke, W., Yarkony, D. R., Köppel, H., Eds.; World Scientific: Singapore, 2004; Vol. 15.
(42) Turro N. J.; Rumamurthy V.; Scaiano J. *Modern Molecular Photochemistry of Organic Molecules*; University Science Books: Sausalito, CA, 2010.
(43) Bearpark, M. J.; Robb, M. A.; Schlegel, H. B. *Chem. Phys. Lett.* **1994**, *223*, 269.
(44) Manaa, M. R.; Yarkony, D. R. *J. Am. Chem. Soc.* **1994**, *116*, 11444.
(45) Dallos, M.; Lischka, H.; Szalay, P.; Shepard, R.; Yarkony, D. R. *J. Chem. Phys.* **2004**, *120*, 7330.
(46) Levine, B. G.; Coe, J. D.; Martínez, T. J. *J. Phys. Chem. B* **2008**, *112*, 405.
(47) Sicilia, F.; Blancafort, L.; Bearpark, M.; Robb, M. *J. Chem. Theory Comput.* **2008**, *4*, 257.

(48) Atchity, G. J.; Xantheas, S. S.; Ruedenberg, K. *J. Chem. Phys.* **1991**, *95*, 1862.
(49) Yarkony, D. R. *J. Phys. Chem. A* **1997**, *101*, 4263.
(50) Paterson, M. J.; Bearpark, M. J.; Robb, M. A.; Blancafort, L. *J. Chem. Phys.* **2004**, *121*, 11562.
(51) Lasome, B.; Siciia, F.; Bearpark, M. J.; Robb, M. A.; Worth, G. A.; Blancafort, L. *J. Chem. Phys.* **2008**, *128*, 124307(10 pages).
(52) Lischka, H.; Dallos, M.; Szalay, P.; Yarkony, D. R.; Shepard, R. *J. Chem. Phys.* **2004**, *120*, 7322.
(53) Yamaguchi, Y.; Osamura, Y.; Goddard, J. D.; Schaefer, H. F. *A New Dimension to Quantum Chemistry: Analytic Derivative Methods in ab initio Molecular Electronic Structure Theory*; Oxford University Press: Oxford, U.K., 1994.
(54) Mead, C. A. *J. Chem. Phys.* **1983**, *78*, 807.
(55) Yarkony, D. R. *J. Chem. Phys.* **2005**, *123*, 204101.
(56) Yarkony, D. R. *J. Chem. Phys.* **2001**, *114*, 2601.
(57) Sicilia, F.; Blancafort, L.; Bearpark, M.; Robb, M. *Theor. Chem. Acc.* **2007**, *118*, 241.
(58) Dillon, J. J.; Yarkony, D. R. *J. Chem. Phys.* **2007**, *126*, 124113.
(59) Schuurman, M.; Yarkony, D. R. *J. Chem. Phys.* **2007**, *126*, 044104.
(60) Coe, J. D.; Ong, M. T.; Levine, B. G.; Martinez, T. J. *J. Phys. Chem. A* **2008**, *112*, 12559.
(61) Yarkony, D. R. *Theor. Chem. Acc.* **1997**, *98*, 197.
(62) Yarkony, D. R. *J. Chem. Phys.* **1998**, *109*, 7047.
(63) Yarkony, D. R. *J. Phys. Chem. A* **2001**, *105*, 2642.
(64) Gromov, E. V.; Trofimov, A. B.; Gatti, F.; Köppel, H. *J. Chem. Phys.* **2010**, *133*, 164309.
(65) Bartlett, R. J. In *Modern Electronic Structure Theory*; Yarkony, D. R., Ed.; World Scientific Publishing: Singapore, 1995; Vol. 2.
(66) Köhn, A.; Tajitu, A. *J. Chem. Phys.* **2007**, *127*, 044105.
(67) Gatti, F.; Iung, C. *Phys. Rep.* **2009**, *484*, 1.
(68) Eisfeld, W.; Viel, A. *J. Chem. Phys.* **2005**, *122*, 204317.
(69) Faraji, S.; Koppel, H.; Eisfeld, W.; Mahapatra, S. *Chem. Phys.* **2008**, *347*, 110.
(70) Viel, A.; Eisfeld, W. *J. Chem. Phys.* **2004**, *120*, 4603.
(71) Viel, A.; Eisfeld, W.; Evenhuis, C. R.; Manthe, U. *Chem. Phys.* **2008**, *347*, 331.
(72) Godsi, O.; Evenhuis, C. R.; Collins, M. A. *J. Chem. Phys.* **2006**, *125*, 104105.
(73) Li, Z. H.; Valero, R.; Truhlar, D. G. *Theor. Chem. Acc.* **2007**, *118*, 9.
(74) Zhu, X.; Yarkony, D. R. *J. Chem. Phys.* **2010**, *132*, 104101.
(75) Zhu, X.; Yarkony, D. R. *Mol. Phys.* **2010**, *108*, 2611.
(76) Dillon, J. J.; Yarkony, D. R.; Schuurman, M. S. *J. Chem. Phys.* **2011**, *134*, 044101.
(77) Mahapatra, S.; Worth, G. A.; Meyer, H.-D.; Cederbaum, L. S.; Köppel, H. *J. Phys. Chem. A* **2001**, *105*, 5567.
(78) Mahapatra, S.; Vallet, V.; Woywod, C.; Köppel, H.; Domcke, W. *Chem. Phys.* **2004**, *304*, 17.
(79) Ichino, T.; Gianola, A. J.; Lineberger, W. C.; Stanton, J. F. *J. Chem. Phys.* **2006**, *125*, 084312.
(80) Papas, B. N.; Schuurman, M. S.; Yarkony, D. R. *J. Chem. Phys.* **2008**, *129*, 124104.
(81) Opalka, D.; Domcke, W. *J. Chem. Phys.* **2010**, *132*, 154108.
(82) Thompson, T. C.; Izmirlian, G.; Lemon, S. J.; Truhlar, D. G.; Mead, C. A. *J. Chem. Phys.* **1985**, *82*, 5597.
(83) Varandas, A. J. C.; Brown, F. B.; Mead, C. A.; Truhlar, D. G.; Blais, N. C. *J. Chem. Phys.* **1987**, *86*, 6258.
(84) Nakamura, H.; Truhlar, D. G. *J. Chem. Phys.* **2002**, *117*, 5576.
(85) Nakamura, H.; Truhlar, D. G. *J. Chem. Phys.* **2003**, *118*, 6816.
(86) Atchity, G. J.; Ruedenberg, K. *Theor. Chem. Acc.* **1997**, *97*, 47.
(87) Pacher, T.; Cederbaum, L. S.; Köppel, H. *J. Chem. Phys.* **1991**, *95*, 6668.
(88) Evenhuis, C. R.; Collins, M. A. *J. Chem. Phys.* **2004**, *121*, 2515.
(89) Evenhuis, C. R.; Lin, X.; Zhang, D. H.; Yarkony, D. R.; Collins, M. A. *J. Chem. Phys.* **2005**, *123*, 134110.
(90) Müeller, H.; Köppel, H.; Cederbaum, L. S. *J. Chem. Phys.* **1994**, *101*, 10263.
(91) Wang, Z.; Kerkines, I. S. K.; Morokuma, K.; Zhang, P. *J. Chem. Phys.* **2009**, *130*, 044313.
(92) Zhu, X.; Yarkony, D. R. *J. Chem. Phys.* **2011**manuscipt in preparation.
(93) Fogarasi, G.; Zhou, X.; Taylor, P. W.; Pulay, P. *J. Am. Chem. Soc.* **1992**, *114*, 8191.
(94) Longuet-Higgins, H. C. *Mol. Phys.* **1963**, *6*, 445.
(95) Bunker, P. R. *Molecular Symmetry and Spectroscopy*; Academic Press: New York, 1979.
(96) Hougen, J. T. *J. Mol. Spectrosc.* **2009**, *256*, 170.
(97) Braams, B. J.; Bowman, J. M. *Int. Rev. Phys. Chem.* **2009**, *28*, 577.
(98) Papas, B. N.; Schuurman, M. S.; Yarkony, D. R. *J. Chem. Phys.* **2009**, *130*, 064306.
(99) Dillon, J. J.; Yarkony, D. R. *J. Chem. Phys.* **2009**, *130*, 154312.
(100) Dillon, J. J.; Yarkony, D. R. *J. Chem. Phys.* **2009**, *131*, 134303.
(101) Dillon, J.; Yarkony, D. R.; Schuurman, M. S. *J. Chem. Phys.* **2011**, *134*, 184314.
(102) Ben-Nun, M.; Martinez, T. J. *J. Phys. Chem. A* **2000**, *104*, 5161.
(103) Beck, M.; Jackle, A.; Worth, G. A.; Meyer, H.-D. *Phys. Rep* **2000**, *324*, 1.
(104) Worth, G. A.; Meyer, H.-D.; Cederbaum, L. S. In *Conical Intersections: Electronic Structure. Dynamics and Spectroscopy*; Domcke, W., Yarkony, D. R., Köppel, H., Eds.; World Scientific: Hackensack, NJ, 2004; Vol. 15.
(105) Worth, G. A.; Meyer, H.-D.; Köppel, H.; Cederbaum, L. S.; Burghardt, I. *Int. Rev. Phys. Chem.* **2008**, *27*, 569.
(106) Worth, G. A.; Robb, M. A.; Burghardt, I. *Faraday Discuss.* **2004**, *127*, 307.
(107) Worth, G. A.; Robb, M. A.; Lasorne, B. *Mol. Phys.* **2008**, *106*, 2077.
(108) Chen, X.; Batista, V. S. *J. Chem. Phys.* **2006**, *125*, 124313.
(109) Tully, J. C. *J. Chem. Phys.* **1990**, *93*, 1061.
(110) Bonhommeau, D.; Valero, R.; Truhlar, D. G.; Jasper, A. W. *J. Chem. Phys.* **2009**, *130*, 234303.
(111) Ananth, N.; Venkataraman, C.; Miller, W. H. *J. Chem. Phys.* **2007**, *127*, 084114.
(112) Miller, W. H. *J. Phys. Chem. A* **2009**, *113*, 1405.
(113) Wodtke, A. M.; Tully, J. C.; Auerbach, D. J. *Int. Rev. Phys. Chem.* **2004**, *23*, 513.
(114) Stier, W.; Prezhdo, O. V. *J. Phys. Chem. B* **2002**, *106*, 8047.
(115) Duncan, W. R.; Stier, W. M.; Prezhdo, O. V. *J. Am. Chem. Soc.* **2005**, *127*, 7941.
(116) Oregan, B.; Grätzel, M. *Nature* **1991**, *353*, 6346.
(117) Roy, S.; Shenvi, N.; Tully, J. C. *J. Phys. Chem. C* **2009**, *113*, 16311.
(118) Pellow, R.; Vala, M. *J. Chem. Phys.* **1989**, *90*, 5612.
(119) Sohlberg, K.; Yarkony, D. R. *J. Phys. Chem. A* **1997**, *101*, 3166.
(120) Sohlberg, K.; Yarkony, D. R. *J. Chem. Phys.* **1997**, *107*, 7690.
(121) Sohlberg, K.; Yarkony, D. R. *J. Chem. Phys.* **1999**, *111*, 3070.
(122) Head-Gordon, M.; Tully, J. C. *J. Chem. Phys.* **1992**, *96*, 3939.
(123) Head-Gordon, M.; Tully, J. C. *Phys Rev. B* **1992**, *46*, 1853.
(124) Gadsuk, J. W. *J. Chem. Phys.* **1983**, *79*, 6341.
(125) Shenvi, N.; Roy, S.; Tully, J. C. *J. Chem. Phys.* **2009**, *130*, 174107.
(126) Wodtke, A. M.; Yuhui, H.; Auerbach, D. J. *Chem. Phys. Lett.* **2005**, *413*, 326.
(127) Gindensperger, E.; Burghardt, I.; Cederbaum, L. S. *J. Chem. Phys.* **2006**, *124*, 144103.
(128) Gindensperger, E.; Burghardt, I.; Cederbaum, L. S. *J. Chem. Phys.* **2006**, *124*, 144104.
(129) Cattarius, C.; Worth, G. A.; Meyer, H. D. *J. Chem. Phys.* **2001**, *115*, 2088.
(130) Warshel, A.; Levitt, M. *J. Mol. Biol.* **1976**, *103*, 227.
(131) Field, M.; Bash, P.; Karplus, M. J. *J. Comput. Chem.* **1990**, *11*, 700.
(132) Singh, U. C.; Kollman, P. A. *J. Comput. Chem.* **1986**, *7*, 718.
(133) Virshup, A. M.; Punwong, C.; Pogorelov, T. V.; Linquist, B. A.; Ko, C.; Martínez, T. J. *J. Phys. Chem. B* **2009**, *113*, 3280.
(134) Slavícek, P.; Martínez, T. J. *J. Chem. Phys.* **2006**, *124*, 084107.

(135) Hoffman, B. C.; Yarkony, D. R. *J. Chem. Phys.* **2000**, *113*, 10091.
(136) Thanopulos, I.; Shapiro, M. *J. Phys. B: At., Mol. Opt. Phys.* **2008**, *41*, 074010.
(137) Abe, M.; Ohtsuki, Y.; Fujimura, Y.; Domcke, W. *J. Chem. Phys.* **2005**, *123*, 064313.
(138) Flores, S. C.; Batista, V. *J. Phys. Chem. B* **2004**, *108*, 6745.
(139) Deb, S.; Weber, P. M. *Annu. Rev. Phys. Chem.* **2011**, *62*, 19.
(140) Hofmann, A.; de VIvie-Riedle, R. *J. Chem. Phys.* **2000**, *112*, 5054.
(141) Hofmann, A.; de VIvie-Riedle, R. *Chem. Phys. Lett.* **2001**, *346*, 299.
(142) Jacobs, H. J. C.; Havinga, E. In *Adv. in Photochemistry*; Pitts, J. N., Hammond, S. G., Gollnick, K., Eds.; J. Wiley: New York, 1979.
(143) Tamura, H.; Nanbu, S.; Ishida, T.; Nakamura, H. *J. Chem. Phys.* **2006**, *124*, 084313.
(144) Tamura, H.; Nanbu, S.; Ishida, T.; Nakamura, H. *J. Chem. Phys.* **2006**, *125*, 034307.
(145) Kondorskiy, A.; Nanbu, S.; Teranishi, Y.; Nakamura, H. *J. Phys. Chem. A* 2010, *114*, 6171.
(146) Bach, A.; Hutchison, J. M.; Holiday, R. J.; Crim, F. F. *J. Chem. Phys.* **2003**, *118*, 7144.
(147) Bach, A.; Hutchison, J. M.; Holiday, R. J.; Crim, F. F. *J. Chem. Phys.* **2002**, *116*, 4955.
(148) Hause, M. L.; Yoon, Y. H.; Crim, F. F. *J. Chem. Phys.* **2006**, *125*, 174309.
(149) Nangia, S.; Truhlar, D. G. *J. Chem. Phys.* **2006**, *124*, 124309.
(150) Lai, W.; Lin, S. Y.; Xie, D.; Guo, H. *J. Chem. Phys.* **2010**, *129*, 154311.
(151) Christopher, P. S.; Shapiro, M.; Brumer, P. *J. Chem. Phys.* **2005**, *123*, 064313.
(152) Sobolewski, A. L.; Domcke, W. *J. Phys. Chem. A* **2007**, *111*, 11725.
(153) Groenhof, G.; Boxin-Cademartory, M.; Hess, B.; Visser, S. D.; Beredsen, H.; Olivucci, M.; Mark, A.; Robb, M. *J. Am. Chem. Soc.* **2004**, *126*, 4228.
(154) Groenhof, G.; Schaefer, L. V.; Boggio-Pasqua, M.; Grubmueller, H.; Robb, M. *J. Am. Chem. Soc.* **2008**, *130*, 3250.
(155) Ko, C.; Virshup, A. M.; Martinez, T. *Chem. Phys. Lett.* **2008**, *460*, 272.
(156) Neumark, D. M. *Annu. Rev. Phys. Chem.* **2001**, *52*, 255.
(157) Continetti, R. *Annu. Rev. Phys. Chem.* **2001**, *52*, 165.
(158) Seidman, T. *Annu. Rev. Phys. Chem.* **2002**, *53*, 41.
(159) Reid, K. L. *Annu. Rev. Phys. Chem.* **2003**, *54*, 397.
(160) Stolow, A. *Annu. Rev. Phys. Chem.* **2003**, *54*, 89.
(161) Reid, K. L. *Int. Rev. Phys. Chem* **2008**, *27*, 607.
(162) Stolow, A.; Underwood, J. G. *Adv. Chem. Phys.* **2008**, *139*, 497.
(163) Neumark, D. M. *J. Phys. Chem. A* **2008**, *112*, 13287.
(164) Hudock, H. R.; Martinez, T. *ChemPhysChem* **2008**, *9*, 2486.
(165) Schuurman, M. S.; Young, R. A.; Yarkony, D. R. *Chem. Phys.* **2008**, *347*, 57.
(166) Duschinsky, F. *Acta Physicochim. V.R.S.S.* **1937**, *1*, 551.
(167) Small, G. J. *J. Chem. Phys.* **1971**, *54*, 3300.
(168) Doktorov, E. V.; Malkin, I. A.; Man'ko, V. I. *J. Mol. Spectrosc.* **1975**, *56*, 1.
(169) Doktorov, E. V.; Malkin, I. A.; Man'ko, V. I. *J. Mol. Spectrosc.* **1977**, *64*, 302.
(170) Gruner, D.; Brumer, P. *Chem. Phys. Lett.* **1987**, *138*, 310.
(171) Hazra, A.; Nooijen, M. *Int. J. Quantum Chem.* **2003**, *95*, 643.
(172) Kupka, H.; Cribb, P. H. *J. Chem. Phys.* **1986**, *85*, 1303.
(173) Ruhoff, P. T.; Ratner, M. A. *Int. J. Quantum Chem.* **2000**, *77*, 383.
(174) Schuurman, M. S.; Yarkony, D. R. *J. Chem. Phys.* **2008**, *128*, 044119.
(175) Reed, K. J.; Zimmerman, A. H.; Anderson, H. C.; Brauman, J. I. *J. Chem. Phys.* **1976**, *64*, 1368.
(176) Oana, C. M.; Krylov, A. I. *J. Chem. Phys.* **2007**, *127*, 234106.
(177) Oana, C. M.; Krylov, A. I. *J. Chem. Phys.* **2009**, *131*, 124114.
(178) Han, S.; Yarkony, D. R. *J. Chem. Phys.* **2010**, *133*, 194107.
(179) Han, S.; Yarkony, D. R. *J. Chem. Phys.* **2011**, *134*, 134110.
(180) Rescigno, T. M.; Lengsfield, B. H., III; McCurdy, C. W. In *Modern Electronic Structure Theory*; Yarkony, D. R., Ed.; World Scientific Publishing: Singapore, 1995.
(181) Lucchese, R. R.; Raseev, G.; McKoy, V. *Phys. Rev. A* **1982**, *25*, 2572.
(182) Winstead, C.; McKoy, V. In *Modern Electronic Structure Theory*; Yarkony, D. R., Ed.; World Scientific Publishing: Singapore, 1995.
(183) Tennyson, J. *Phys. Rep.* **2010**, *491*, 29.
(184) Langhoff, S. R.; Kern, C. W. In *Modern Theoretical Chemistry*; Schaefer, H. F., Ed.; Plenum: New York, 1977; Vol. 4.
(185) Mishra, S.; Poluyanov, L. V.; Domcke, W. *J. Chem. Phys.* **2007**, *126*, 134312.
(186) Poluyanov, L. V.; Domcke, W. *J. Chem. Phys.* **2008**, *129*, 224102.
(187) Mead, C. A. *Chem. Phys.* **1980**, *49*, 33.
(188) Schuurman, M. S.; Weinberg, D. E.; Yarkony, D. R. *J. Chem. Phys.* **2007**, *127*, 104309.
(189) Ham, F. S. *Phys. Rev.* **1965**, *138*, A1727.
(190) Bersuker, I. *The Jahn-Teller Effect*; Cambridge University Press: Cambridge, U.K., 2006.
(191) Ramond, T. M.; Davico, G. E.; Schwartz, R. L.; Lineberger, W. C. *J. Chem. Phys.* **2000**, *112*, 1158.
(192) Jin, J.; Sioutis, I.; Tarczay, G.; Gopalakrishnan, S.; Bezanat, A.; Miller, T. A. *J. Chem. Phys.* **2004**, *121*, 11780.
(193) Neumark, D. Private communication, 2009.
(194) Huber, K. P.; Herzberg, G. *Molecular Spectra and Molecular Structure. IV. Constants of Diatomic Molecules*; Van Nostrand Reinhold: New York, 1979.
(195) Brossard, S. D.; Carrick, P. G.; Chappell, E. L.; Hulegaard, S. C.; Engelking, P. C. *J. Chem. Phys.* **1986**, *84*, 2459.
(196) Misra, P.; Zhu, X.; Hsueh, C.-Y.; Halpern, J. B. *Chem. Phys.* **1993**, *178*, 377.
(197) Lee, Y.-Y.; Wann, G.-H.; Lee, Y.-P. *J. Chem. Phys.* **1993**, *99*, 9465.
(198) Applegate, B. E.; Bezant, A. J.; Miller, T. A. *J. Chem. Phys.* **2001**, *114*, 4869.
(199) Applegate, B. E.; Miller, T. A.; Barckholtz, T. A. *J. Chem. Phys.* **2001**, *114*, 4855.
(200) Ichino, T.; Wren, S. W.; Vogelhuber, K. M.; Gianola, A. J.; Lineberger, W. C.; Stanton, J. F. *J. Chem. Phys.* **2008**, *129*, 084310.
(201) Matsika, S.; Yarkony, D. R. *J. Am. Chem. Soc.* **2003**, *125*, 12428.
(202) Schuurman, M. S.; Yarkony, D. R. *J. Chem. Phys.* **2008**, *129*, 064304.
(203) Motzke, A.; Lan, Z.; Woywod, C.; Domcke, W. *Chem. Phys.* **2006**, *329*, 50.
(204) Zhu, X.; Yarkony, D. R. *J. Phys. Chem. C* **2010**, *114*, 5312.
(205) Huang, P.; Carter, E. A. *Nano Lett.* **2006**, *6*, 1146.
(206) Davis, A. V.; Wester, R.; Bragg, A. E.; Neumark, D. M. *J. Chem. Phys.* **2003**, *118*, 999.
(207) Surber, E.; Sanov, A. *J. Chem. Phys.* **2002**, *116*, 5921.
(208) Rathbone, G. J.; Sanford, T.; Andrews, D.; Lineberger, W. C. *Chem. Phys. Lett.* **2005**, *401*, 570.